

Metro WDM Networks: Performance Comparison of Slotted Ring and AWG Star Networks

Hyo-Sik Yang, Martin Herzog, Martin Maier, and Martin Reisslein

Abstract

Both WDM networks with a ring architecture and WDM networks with a star architecture have been extensively studied as solutions to the ever increasing amount of traffic in the metropolitan area. Studies typically focus on either the ring or the star and significant advances have been made in the protocol design and performance optimization for the WDM ring and the WDM star, respectively. However, very little is known about the relative performance comparisons of ring and star networks. In this study we conduct a comprehensive comparison of a state-of-the-art WDM ring network with a state-of-the-art WDM star network. In particular, we compare time-slotted WDM ring networks (both single-fiber and dual-fiber) with tunable-transmitter and fixed-receiver (TT-FR) nodes and an AWG based single-hop star network with tunable-transmitter and tunable-receiver (TT-TR) nodes. We evaluate mean aggregate throughput, relative packet loss, and mean delay by means of simulation for Bernoulli and self-similar traffic models for unicast traffic with uniform and hot-spot traffic matrices as well as for multicast traffic. Our results quantify the fundamental performance characteristics of ring networks vs. star networks and vice versa, as well as their respective performance limiting bottlenecks, and thus provide guidance for directing future research efforts.

I. INTRODUCTION

Today's metropolitan area networks (MANs) are mostly SONET/SDH ring networks which suffer from a number of drawbacks. Due to their voice-centric TDM operation and symmetric circuit provisioning bursty asymmetric data traffic is supported only very inefficiently. Furthermore, SONET/SDH equipment is quite expensive and significantly decreases the margins in the cost-sensitive metro market. This prevents new companies from entering the metro market. The inefficiencies of SONET/SDH ring networks create a severe bandwidth bottleneck at the metro level. The resultant so-called *metro gap* prevents high-speed clients, e.g., Gigabit Ethernet, from tapping into the vast amounts of bandwidth available in the backbone [1]. In order to (i) bridge this bandwidth abyss between high-speed clients and backbone, (ii) enable new applications benefiting from the huge amounts of bandwidth available in the backbone, and (iii) stimulate revenue growth, more efficient and cost-effective metro architectures and protocols are needed [2].

Wavelength division multiplexing (WDM) networks have been extensively investigated as solutions to the metro gap. As discussed in more detail in Section I-A, studies typically focus on either the ring

H.-S. Yang is with the Dept. of Electrical Engineering, Arizona State University (e-mail: yangkoon@asu.edu)

M. Herzog is with the Telecommunication Networks Group, Technical University Berlin, 10587 Berlin, Germany, (e-mail: herzog@tkn.tu-berlin.de).

M. Maier is with the Centre Tecnològic de Telecomunicacions de Catalunya (CTTC), Barcelona, Spain, (e-mail: martin.maier@cttc.es).

Corresponding Author: M. Reisslein is with the Dept. of Electrical Engineering, Arizona State University, Goldwater Center, MC 5706, Tempe, AZ, 85287-5706, Phone: (480)965-8593, Fax: (480)965-8325, (e-mail: reisslein@asu.edu, web: <http://www.fulton.asu.edu/~mre>).

[3] or the star topology [4], [5] and significant advances have been made in the medium access control (MAC) protocol design and performance optimization of the WDM ring and the WDM star, respectively. However, very little is known about the relative performance comparison of ring and star networks. In this paper, we conduct a comprehensive comparison of state-of-the-art ring and state-of-the-art star metro WDM networks. Our findings reveal the respective strengths and weaknesses of ring networks and star networks. We also identify the bottlenecks that limit the ring/star performance.

In our study we focus on the performance metrics throughput and delay, which are evaluated for the individual source-destination node pairs as well as aggregated (averaged) for the entire network. We also examine the relative packet loss for the individual source-destination node pairs as well as aggregated for the network. We note that aside from these packet level metrics, metro WDM networks could be evaluated for a number of other metrics, such as call level performance (call blocking probability) for networks that allow for a mix of packet and circuit switched traffic. Also, the capital and operational expenditures could be interesting metrics for comparison. In addition, the network survivability and protection in the face of equipment and/or fiber failures are important aspects of metro WDM networks. Both ring networks and star networks require protection which can be achieved with dual-fiber rings in ring networks and components in parallel to the star hub, as studied in [6]–[8], in star networks. Comparing the relative performance tradeoffs of these protection strategies for metro WDM ring and star networks is beyond the scope of this paper. In this to the best of our knowledge first relative performance comparison of ring and star WDM networks we focus on the elementary packet level metrics to get a first understanding of the relative ring and star strengths and weaknesses.

This paper is structured as follows. In the following subsection we review related work. In Section II, we describe the architectures and medium access control (MAC) protocols of the considered single-fiber and dual-fiber ring networks. In Section III, we describe the architecture and MAC protocol of the considered arrayed-waveguide grating (AWG) based star network. In Section IV, we present our comparative simulations of ring and star WDM networks. We consider uniform and non-uniform traffic matrices for Bernoulli and self-similar traffic. We study the impact of fairness control on the performance of ring networks. We also compare the performance of ring and star networks for multicasting traffic. We summarize our findings in Section V.

A. Related Work

In this section, we give an overview of the existing literature on (i) ring WDM networks, (ii) star WDM networks, and (iii) relative performance comparisons of different types of WDM networks. Ring WDM networks consist either of a single-fiber ring (as considered in most studies) or a dual-fiber ring, see for instance [9]. The nodes are equipped with either one fixed-tuned transmitter and an array of fixed-tuned receivers (FT–FR^Λ) [10], an array of fixed-tuned transmitters and one fixed-tuned receiver (FT^Λ–FR) [11], [12], or two arrays of fixed-tuned transmitters and fixed-tuned receivers (FT^Λ–FR^Λ) [13], [14], where Λ denotes the number of wavelengths in the system. Alternatively, the array of fixed-tuned transceivers can

be replaced with one tunable device, e.g., a TT–FR node structure [15]. For cost and scalability reasons it is generally desirable to deploy a small number of transceivers at each node and decouple the number of wavelengths from the number of nodes. Therefore, we consider ring networks in which each node is equipped with one single transceiver and each wavelength is shared by multiple nodes [16], [17], as described in greater detail in Section II.

Most star WDM networks for the metro area are based on the broadcast-and-select passive star coupler (PSC) [4], [5]. Star WDM networks based on the wavelength-routing arrayed-waveguide grating (AWG) have recently attracted attention both for metropolitan area networks [18]–[21] and national-scale networks [22], [23]. It was shown in [24] that arrayed-waveguide grating (AWG) based single-hop networks clearly outperform their PSC based counterparts in terms of throughput, delay, and packet loss due to spatial wavelength reuse. Therefore, in our comparison we consider a single-hop star WDM network that is based on a wavelength-routing AWG, as outlined in Section III.

The relative performance comparison of WDM networks with different topologies has received very little attention so far. We are only aware of the delay comparison between ring and bus networks [25].

II. SLOTTED RING WDM NETWORK

A. Network Architecture

In this section, we describe the basic architecture of an all-optical WDM ring network with N nodes and Λ logical wavelength channels and a TT–FR node structure. We consider initially the single-fiber network which connects all nodes with a single unidirectional fiber [17] and then the dual-fiber network which connects all nodes with two counter-directional fibers [9]. In the single-fiber network, the fiber bandwidth is divided into Λ wavelength channels. Each channel is divided into fixed-length time slots whose boundaries are synchronized across all wavelengths. The slot duration equals the transmission time of a fixed-size packet. (We note that variable-size packets can be accommodated on ring networks using for instance the mechanisms studied in [9].) Each node is equipped with one tunable transmitter and one fixed-tuned receiver (TT–FR). A node can send packets on any wavelength, while it is able to receive packets only on a preassigned *drop wavelength*. For $N = \Lambda$ each node has its own separate *home channel* for reception, as shown in Fig. 1 for $N = \Lambda = 4$. For $N > \Lambda$ each wavelength is shared by several nodes for the reception of packets. Specifically, the destination nodes $j = i + n \cdot \Lambda$ with $n \in \{0, 1, \dots, \lceil \frac{N}{\Lambda} \rceil - 1\}$ share the same drop wavelength i , $i \in \{1, 2, \dots, \Lambda\}$. Consequently, nodes sharing the same drop wavelength have to forward packets toward the destination node, resulting in *multihopping*. The destination node takes the packet from the ring (destination stripping). With this destination stripping, wavelengths can be *spatially reused* by downstream nodes, leading to an increased network capacity. To avoid head-of-line (HOL) blocking each node deploys $(N - 1)$ *virtual output queues* (VOQs), one for each destination node. Each VOQ holds up to B packets.

In the dual-fiber ring network, the N nodes are interconnected with two counter-directional fiber rings, as illustrated in Fig. 2. To investigate the effect of the counter-directionality in the fibers we assign $\Lambda/2$

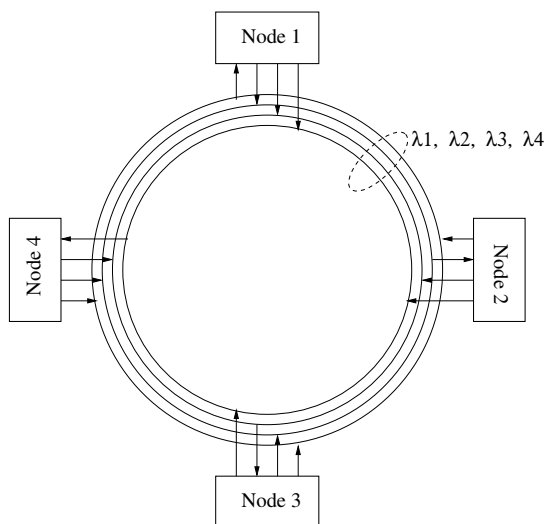


Fig. 1. Single-fiber network architecture with $N = 4$ nodes and $\Lambda = 4$ wavelength channels.

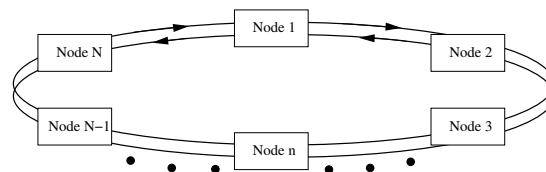


Fig. 2. Dual-fiber ring network architecture.

wavelength channels to each fiber, for a total of Λ channels, as in the single-fiber ring network. In a dual-fiber network the node structure of the single-fiber network is typically duplicated, i.e., there are one TT and one FR for each fiber [9]. The TT^2 - FR^2 node structure allows a node to send and to receive two packets simultaneously. Each node has a home channel on each of the fibers.

B. MAC Protocol

In this section we outline the medium access control (MAC) protocol employed in the considered ring networks. To control the access of the nodes to the slots on the wavelength channels, every slot on each wavelength is accompanied by control information. This control information indicates whether the slot is empty or occupied by a data packet (wavelength availability information). If the slot is occupied, the control information also gives the destination address of the packet occupying the slot. The control information may be transmitted on a separate control channel (as for instance in [9], [26], [27]) or in a subcarrier multiplexed header (as for instance in [16], [28]). We describe the principles of the control information transmission by discussing the control channel approach. For details on the subcarrier multiplexing approach we refer the interested reader to the corresponding references. With the control channel approach, the control information in a given slot on the control channel corresponds to the status of the data wavelength channels in the next slot. This is illustrated for the wavelength availability information (bits) in Fig. 3. (The destination node information is not shown to avoid overcrowding this illustrative figure.) If a bit is set to one the corresponding wavelength channel is occupied in the next slot, and otherwise it is empty.

We note that with the control channel approach there is an additional wavelength channel for control on each fiber, for a combined total of $\Lambda + 1$ wavelength channels in the single-fiber ring network and $\Lambda + 2$ wavelength channels in the dual-fiber ring network. In addition, there is a fixed-tuned transceiver (FT-FR)

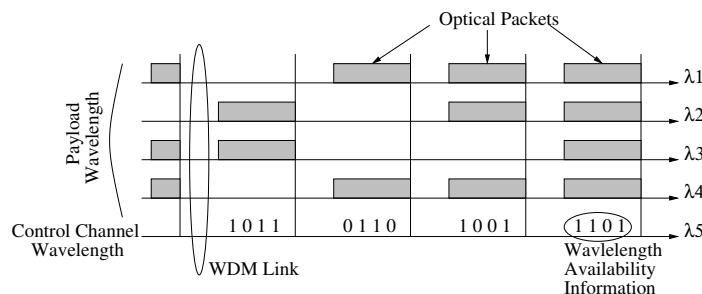


Fig. 3. Control information transport on control channel: control information in a slot corresponds to data (payload) wavelength occupancy in next slot.

at each node for each fiber to transmit and monitor the control information on the control channel on each fiber.

For the packet transmission, we consider the so-called *a posteriori* access strategy, which we outline at first for the single-fiber to highlight the main points. With the *a posteriori* access strategy, a node first checks the availability status of each slot on all wavelengths by inspecting the control information and then selects the appropriate VOQ. (This *a posteriori* strategy gives generally better performance at the expense of higher complexity compared with the *a priori* access strategy [17].) The node has to wait until an empty slot arrives on one (or more) wavelength channel(s). When an arriving slot is empty on one (or more) wavelength channel(s) the node can use this slot to transmit one packet from one of the corresponding VOQs. In the considered single-fiber ring architecture with per-destination VOQs, buffer selection is necessary if (i) $N = \Lambda$ and multiple channels have an empty slot, or if (ii) $N \geq \Lambda$ and at least one channel has an empty slots since a node can only transmit one packet at any given time with its single transmitter. Among various buffer selection schemes we choose the *longest queue (LQ)* selection scheme. With the LQ scheme, the longest VOQ (i.e., VOQ with the largest occupancy) is chosen. When there is a tie, the queue with the lowest index $j \in \{1, 2, \dots, (N - 1)\}$ is chosen. The motivation behind this LQ scheme is load balancing among the queues in the system, which increases the node and network throughput at acceptable system complexity [17].

In the dual-fiber ring network, the packets are transmitted in similar fashion with the *a posteriori* access strategy. The two main adaptations of the access strategy outlined for the single-fiber network to the dual-fiber network are (i) that a node can transmit up to two packets simultaneously, and (ii) that a packet can be transmitted in either direction along the ring. Different strategies for choosing the direction are studied in Section IV-B.

We remark that the packet transmissions according to the wavelength availabilities require fast-tunable transmitters with a tuning time that is a small fraction of the slot duration, which is on the order of a few microseconds for typical scenarios, see IV-A. This requirement will be fulfilled by the recently reported fast-tunable transmitters with tuning times on the order of a few nanoseconds, see for instance [29], [30].

III. AWG BASED STAR WDM NETWORK

A. Network Architecture

As shown in Fig. 4, the star network is based on a $D \times D$ AWG used as a wavelength-routing device. A wavelength-insensitive $S \times 1$ combiner is attached to each AWG input port and a wavelength-insensitive $1 \times S$ splitter is attached to each AWG output port. Thus, the network connects $N = D \cdot S$ nodes. Each node is equipped with a laser diode (LD) and a photodiode (PD) for data transmission and reception, respectively. Both data transmitter and receiver are tunable over Λ wavelengths which are not preassigned to nodes (TT-TR). Similar to the ring network, each node has $(N - 1)$ VOQs, one for each destination. Again, each VOQ holds up to B packets.

The number of available wavelengths Λ span R adjacent free spectral ranges (FSRs) of the underlying AWG, each FSR consists of D contiguous wavelength channels, i.e., $\Lambda = R \cdot D$, as illustrated in Fig. 5. Note that the AWG allows for spatial wavelength reuse. As a result, the Λ wavelengths can be simultaneously applied at each of D AWG input ports, for a total of $D \cdot \Lambda$ wavelength channels connecting the D AWG input ports with the D AWG output ports. Also, note that there are R wavelength channels connecting each AWG input-output port pair.

The MAC protocol makes use of a control channel to broadcast control information. This control channel can be implemented (i) as an inband control channel by exploiting the spectral slicing of a broadband light source in conjunction with spectrum spreading of the control signals [18], or (ii) as an out-of-band control channel, e.g., by running a PSC in parallel to the AWG [8].

1) *Inband Signaling*: Each node deploys a broadband light source, e.g., light emitting diode (LED), for broadcasting the control information. The LED signal is *spectrally sliced* by the wavelength-routing

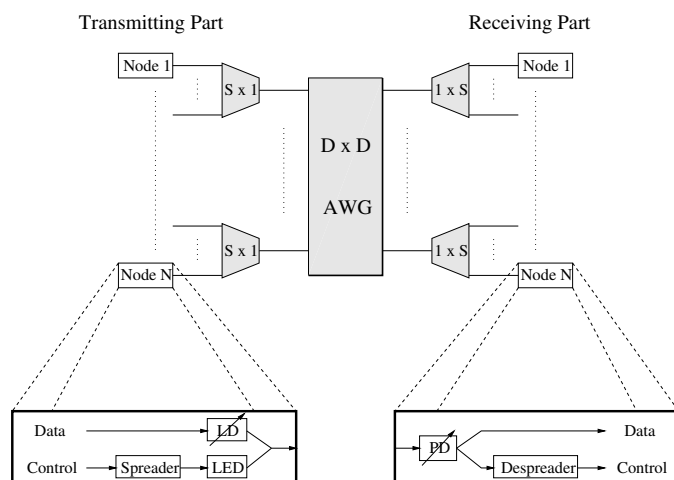


Fig. 4. Architecture of AWG based star WDM network.

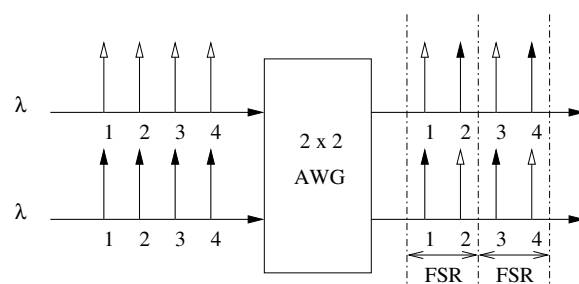


Fig. 5. Illustration of wavelength routing in AWG with $D = 2$ input and output ports when $R = 2$ FSRs are used. Each FSR provides one wavelength channel between an input-output port pair. A total of $D \cdot D \cdot R = D \cdot \Lambda = 2 \cdot 4$ wavelength channels connect the input ports to the output ports.

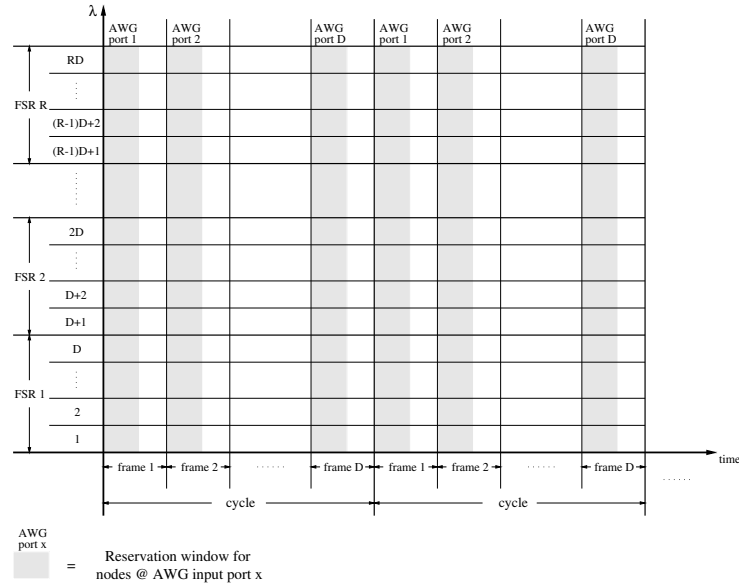


Fig. 6. Timing structure and wavelength assignment in AWG based star network with inband signaling.

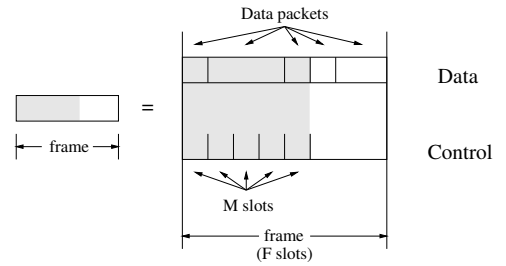


Fig. 7. Frame format in AWG based star network.

AWG such that all receivers obtain the control information. The signaling is done *in-band* using for instance spread spectrum techniques, i.e., LED and LD signals overlap spectrally and are separated in the receiver. With this approach only a single broadband light source and some (electronic) signal processing is required per node. However, it has been shown in [31] that the capacity of an inband control channel using a broadband light source is limited to a few Mbps.

2) *Out-of-band Signaling*: Another option is to deploy a separate out-of-band control channel, e.g., a PSC to which each node is connected via an additional fixed-tuned transceiver and fiber pair could be used in parallel with the AWG. This requires more hardware than the inband signaling approach but the control channel capacity is much higher. Additionally, the PSC part of the network can be used for protection of the single point of failure of star networks, as shown in [8].

B. MAC Protocol

In the considered MAC protocol, wavelengths are assigned dynamically *on demand* such that any pair of nodes is able to communicate in one *single hop*. The applied MAC protocol is an *attempt-and-defer reservation* protocol, i.e., a data packet is sent after a successful reservation, which is conducted with a control packet. The reservation protocol avoids both channel and receiver collisions of data packets. We consider a MAC protocol with data packet aggregation. That is, a single control packet makes a reservation for all (fixed-size) data packets that are destined to a given destination node (i.e., are buffered in the corresponding VOQ), thus forming *variable-size* data packet aggregates. The data packet aggregate is kept in the VOQ until it has been transmitted.

1) *Inband Signaling*: With inband signaling time is divided into cycles, as shown in Fig. 6. Each cycle consists of D frames. Each frame contains F inband (IB) control slots, as illustrated in Fig. 7. Each frame

is partitioned into the first M , $1 \leq M < F$, IB control slots (shaded region) and the remaining $(F - M)$ IB control slots. The length of the IB control slot is equal to the time required to send a control packet (as detailed shortly) over the inband control channel. In the first M IB control slots, control packets are transmitted and all nodes tune their receivers to one of the corresponding LED slices (channels) in order to obtain the control information. To avoid receiver collisions of control packets, all S nodes attached to AWG input port i (via the same combiner) send their control packets in frame i , $1 \leq i \leq D$, of a given cycle. The M IB control slots are not fixed assigned. Instead, control packets are sent on a contention basis using slotted ALOHA. A node is permitted to send up to M control packets in its assigned frame i .

Similar to the ring network, each node deploys the LQ buffer selection scheme (however, opposed to the ring we do not employ an *a posteriori* access strategy in the star). Each node first chooses the VOQ with the largest number of unscheduled packets and randomly selects one of the M IB control slots for sending the corresponding control packet. Next, a control packet is transmitted for the VOQ with the second largest number of unscheduled packets in a randomly selected slot out of the remaining $(M - 1)$ IB control slots. This procedure is repeated until control packets for all but no more than M non-empty VOQs are sent. VOQs for which a control packet is currently on its way (so it is not yet known whether it will be successful or not) are not considered in the LQ selection. To reduce the number of collisions a control packet for a selected VOQ is sent with probability $1/S$.

Control and data are transmitted simultaneously, but only from nodes at a given AWG input port i . In the first M IB control slots of frame i , the nodes at the other AWG input ports cannot transmit since each node's single receiver is not able to pick up control packets sent on different wavelength channels. In the last $(F - M)$ IB control slots of each frame no control packets are sent, allowing receivers to be tuned to any arbitrary wavelength. This freedom enables transmissions between any pair of nodes. Thus, data from any AWG input port can be received, allowing for *spatial wavelength reuse*.

After half the end-to-end round-trip time every node (including the sending node) collects all control packets by locking its receiver to one of the LED slices carrying the control information during the first M IB control slots of every frame. Thus, each node maintains *global knowledge* of all the other nodes' activities and also learns whether its own control packets collided in the control packet contention or not. All nodes process the successfully received control packets by executing the same first-come-first-served and first-fit scheduling algorithm, which we adopt since scheduling in very-high-speed optical networks must have low complexity. The scheduling algorithm tries to schedule the variable-size data packets within the scheduling window of pre-specified length. If the scheduling fails, the source node retransmits the control packet in the next cycle, provided the corresponding VOQ is still among the M longest VOQs.

2) *Out-of-band Signaling*: With out-of-band signalling, the basic time unit on the control channel is the control slot. The length of the control slot is equal to the time required to send a control packet over the out-of-band control channel. For our comparisons in this paper we consider the following packet transmission strategy with data packet aggregation. Each node employs the LQ buffer selection scheme

to determine for which VOQ to send control packets. More specifically, in each control slot, each node selects the VOQ with the largest number of unscheduled packets, forms a data packet aggregate from the packets, and prepares a corresponding control packet. The control slots for control packet transmission are not fixed assigned. Instead, the control packets are sent on a contention basis using slotted ALOHA. Specifically, a given node sends its prepared control packet with probability $1/N$ in a given control slot.

As with inband signaling after a control packet is received (after half the end-to-end round trip time of the PSC network) all nodes perform the same first-come-first-served-first-fit scheduling algorithm. Since the data receivers are no longer required to periodically tune to a certain wavelength, spatial wavelength reuse is possible all the time.

If the control packet collided in the control packet contention, or the scheduling of the data packet within the scheduling window fails, the source node retransmits the control packet in the next control slot, provided the corresponding VOQ is still the longest VOQ. Also, note that VOQs for which a control packet is currently on its way (so it is not yet known whether it will be successful or not) are not considered in the LQ selection.

IV. PERFORMANCE COMPARISON

In this section, we conduct a detailed quantitative comparison between the state-of-the-art ring and star metro WDM networks described in the preceding two sections. In our performance comparison we focus on the packet level performance metrics, i.e., throughput, packet delay, and packet loss, which we define in Subsection IV-A, in which we also describe our simulation set-up.

Prior to proceeding to our detailed investigations of the packet level performance we briefly note that the ring and star networks have specific advantages and pose specific challenges at the photonics level and for implementation. We briefly review the photonic level issues arising from transmission impairments and insertion losses, which are important considerations for the choice of network topology. In particular, in ring networks, the insertion losses of the wavelength multiplexers and demultiplexers (which are typically based on AWGs) used in all-optical node architectures may limit the power budget and thereby the number of nodes that can be traversed without signal regeneration [32], [33]. Furthermore, ring networks are affected by amplified spontaneous emission (ASE) noise, which may accumulate over long all-optical paths with multiple amplifiers. This accumulated ASE noise along with other impairments, such as fiber nonlinearities and crosstalk, may significantly degrade the signal quality, see for instance [34]. Techniques to mitigate these effects are under development; the ASE noise accumulation, for instance, can be reduced by employing variable optical attenuators [35]. Also, the signal regeneration at a ring node forwarding traffic to other nodes on its drop wavelength can overcome these limitations. In the single-hop star network, on the other hand, the AWG is passed only once between each pair of source and destination nodes. Thus, the insertion loss of the AWG and the transmission impairments do typically not severely restrict the scale of the network, and allow in fact for a national scale single-hop network [31], [36].

Another critical issue for the operation of packet-switched WDM networks is synchronization at the

slot level. Ring networks allow for relatively simple synchronization even at extremely high data rates, see for instance [37]. In star networks, on the other hand, the slot synchronization is more challenging due to the distributed nature of the network nodes and the possibly different distances of the nodes to the hub of the star network. Techniques to achieve synchronization in PSC based star networks have been studied extensively, see for instance [38]–[40] [41, Sec. 7.2.1], and can be extended to the AWG based star network in a straightforward manner.

A. Simulation Set-up and Performance Metrics

By default we consider typical metro networks interconnecting $N = 32, 64$ nodes that are equidistant to each other on the circumference of a ring with a diameter of 91.67 km. The parameters used in both networks are summarized in Table I, those specific to the star are listed in Table II. The nodes are interconnected by a ring WDM network or a star WDM network with $\Lambda = 8$ wavelength channels. (In the dual-ring network there are four wavelength channels on each fiber plus two control wavelength channels, one on each fiber, resulting in a total of 10 wavelength channels.) Each wavelength channel operates at a line rate of 2.5 Gbit/sec (OC48) and the propagation speed on the optical fiber link is set to $2 \cdot 10^5$ km/sec. The packet size is fixed to 1500 bytes, which is one of the dominant packet sizes in the Internet as well as the maximum packet size (maximum transfer unit (MTU)) of Ethernet. The corresponding slot duration is $4.8 \mu\text{sec}$ (1500 byte/2.5 Gbps). Note that in the star network we distinguish between the $4.8\mu\text{sec}$ (data) slots and the IB and OB control slots. It is advantageous to use short control slots, since more control packets can be sent per time unit. The size of a control packet is assumed to be 2 bytes (which is sufficient to accommodate destination address and length of data aggregate). The minimum control slot duration depends on the speed of the control channel. While a line rate of 333 Mbps for the out-of-band control channel is easily feasible, a line rate of 3.33 Mbps for the inband control channel is expected to be technologically feasible within the next few years [31]. Note that with these parameter settings the length of the IB control slot is $4.8\mu\text{sec}$, i.e., equal to the length of the (data) slot.

Bernoulli and self-similar traffic are considered. In both cases, the average packet generation rate at each given node is σ , $0 \leq \sigma \leq 1$. More precisely, at a given node in each slot a new packet is independently generated for each of the other $(N - 1)$ nodes with probability $\sigma/(N - 1)$. A newly generated packet is put in the corresponding VOQ of the destination node (or dropped if the VOQ is full). Similarly, for each of the destination VOQs, self-similar packet traffic with Hurst parameter 0.75 is generated from ON/OFF processes with Pareto distributed on-duration and geometrically distributed off-duration [42]. For both types of traffic the N nodes in the network generate on average $N \cdot \sigma$ packets per slot. In addition to the uniform traffic, where a packet generated by a given node is destined to any one of the other $(N - 1)$ nodes with equal probability $1/(N - 1)$, we consider non-uniform hot-spot traffic in Section IV-C and Section IV-F.

In our performance evaluation we consider the mean aggregate throughput, the relative packet loss, as well as the mean packet delay. The mean aggregate throughput is defined as the mean number of source

TABLE I
NETWORK PARAMETERS: DEFAULT VALUES FOR BOTH
RING AND STAR NETWORK

Description	Symbol	Default Value
Network diameter	Δ	91.67 km
Number of nodes	N	32, 64
Number of wavelengths	Λ	8
Link speed	C	2.5 Gbit/sec
Propagation speed	c	$2 \cdot 10^5$ km/sec
Packet (slot) size	L	1500 Bytes
Slot duration		4.8 μ sec
VOQ size (per dest. node)	B	64 packets

TABLE II
PARAMETERS SPECIFIC TO STAR: DEFAULT VALUES

Description	Symbol	Default Value
Splitter/combiner degree	S	8
Control packet size		2 Byte
	External Control Channel	
AWG degree	D	8
# of used FSRs	R	1
Control channel speed		333 Mbps
OB control slot duration		48 nsec
Scheduling window size		200 slots
	Inband Signaling	
AWG degree	D	4
# of used FSRs	R	2
Control channel speed		3.33 Mbps
IB control slot duration		4.8 μ sec
= slot duration		
Frame length	F	32 slots
# of slots for control per frame	M	16
Scheduling window size		1 cycle = 256 slots

node transmitters sending in the network in steady state. (Note that in the dual-fiber network a source node can transmit up to two packet simultaneously as opposed to the star network with at most one active transmitter per source node.) We also study the mean throughput for individual source-destination node pairs, which equals the probability that the considered source node is transmitting a packet to the considered destination node in steady state. (Note that packets forwarded by intermediate nodes along the ring do not count towards the measured throughput; only the transmission of the original source node contributes to the throughput.)

The relative packet loss in the network is defined as the ratio of the total number of dropped packets and the total number of generated packets in the network. For some scenarios we also study the relative packet loss of individual source-destination node pairs, which is the ratio of the total number of dropped packets of a given source-destination node pair and the total number of packets generated for the source-destination node pair.

We define the mean packet delay in the network as the time period elapsed from the generation of a packet to the complete reception of the packet in msec in steady state.

We estimate the defined performance metrics from discrete event simulations. Each simulation was run for 10^6 slots (including a warm-up phase of 10^5 slots). For Bernoulli traffic we obtained 95% confidence intervals on the performance metrics using the method of batch means. The 95% confidence intervals are too small to be seen in the figures.

B. Uniform (Balanced) Traffic Scenario without Fairness Control

We first compare the performance of the ring and star networks for uniform (balanced) traffic, where a given source node sends a generated packet to any of the remaining $(N - 1)$ nodes with equal probability $1/(N - 1)$. We consider both Bernoulli and self-similar traffic. Performance of ring and star network

without fairness control are shown in Figs. 8 – 13 with $N = 32$ and Figs. 14 – 19 with $N = 64$ for both uniform Bernoulli and self-similar traffic.

In the dual-fiber ring network each packet can be sent on either of the two counter-directional rings. Two algorithms for choosing the direction are compared. With the first algorithm (Alg. 1) a packet is sent in the first empty slot that appears on either of the two rings. In the second algorithm (Alg. 2) the packet is sent on that ring which provides the smaller hop distance to the corresponding destination. While with Alg. 1 the throughput improves only very slightly compared to a single fiber ring, Alg. 2 roughly doubles the number of concurrent transmissions at medium to high traffic loads, as shown in Figs 8 and 14. This is because with Alg. 2 the mean hop distance is reduced by 50% and the spatial wavelength reuse is increased by a factor of two. Note that Alg. 1 achieves a mean delay which is even worse than that in the single-fiber ring due to the increased queueing delay, as shown in Figs 12 and 18.

We use IB signaling with $N = 32$ and use OB signaling with $N = 64$ for star network. For Figs. 15, 17, and 19, we use OB control signal as well as IB signaling for self-similar traffic.

C. Non-uniform (Unbalanced) Traffic Scenario without Fairness Control

We now focus on self-similar traffic and compare the ring and star network performance for a non-uniform (unbalanced) traffic mix consisting of a uniform traffic component and a client-server traffic component. Specifically, we assume to have one hot-spot (either server or point of presence (POP)), while the remaining $(N - 1)$ nodes act as identical clients. A client sends a fraction h of the traffic to the hot-spot, while the remaining fraction $(1 - h)$ of the traffic is equally distributed among the other $(N - 2)$ clients. Note that $h = 1/(N - 1)$ corresponds to uniform traffic only as discussed above. We assume that the server generates as much traffic as all $(N - 1)$ clients together and set $\sigma = 0.4$. Similar to the uniform traffic scenario, the total load offered to the network is $N \cdot \sigma$. The performance results are shown in Figs. 20, 22, and, 24 for $N = 32$ and Figs. 21, 23, and, 25 for $N = 64$. We use IB signaling with $N = 32$ and OB signaling with $N = 64$ for the star network.

Next, we fix $h = 0.3$ and study fairness among the individual source-destination node pairs, with node 1 functioning as server. As shown in Fig. 26, the star network provides throughput fairness among all clients due to the random control packet contention and the first-come-first-served scheduling. The server achieves a larger mean throughput which is desirable since it has much more data to send than the clients. In contrast, Fig. 27 re-confirms the fairness problems in ring networks. The hot-spot, node 1, leaves most slots at its drop-wavelength empty. The succeeding nodes use these slots and achieve a high throughput to the hot-spot at the expense of the nodes further downstream, for which no capacity is left. Only nodes downstream to the nodes which share the same drop wavelength with the hot spot, get a chance to send to the server using free slots.

D. Fairness Control in Ring Network

Due to the ring symmetry and the applied destination release each node has a better-than-average access to channels leading to certain destination nodes and a worse-than-average access to channels leading to

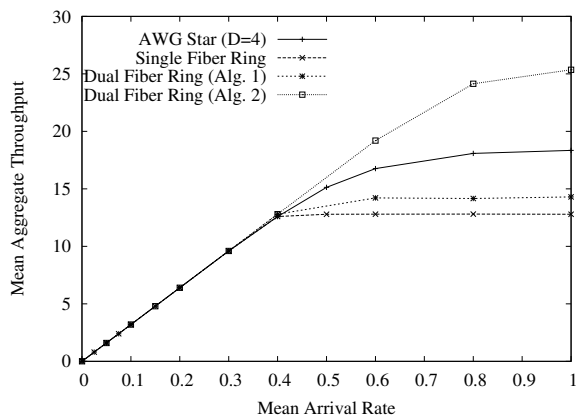


Fig. 8. Mean aggregate throughput for uniform Bernoulli traffic without fairness control, $N = 32$

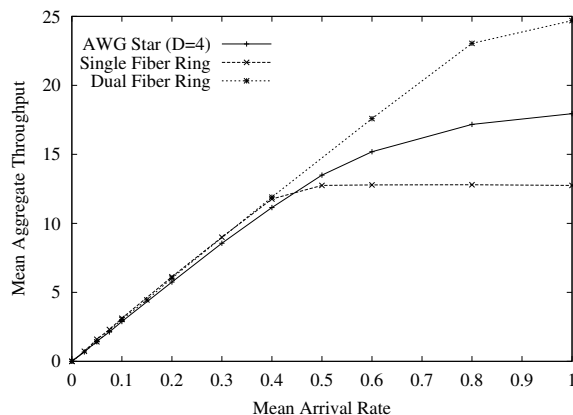


Fig. 9. Mean aggregate throughput for uniform self-similar traffic without fairness control, $N = 32$

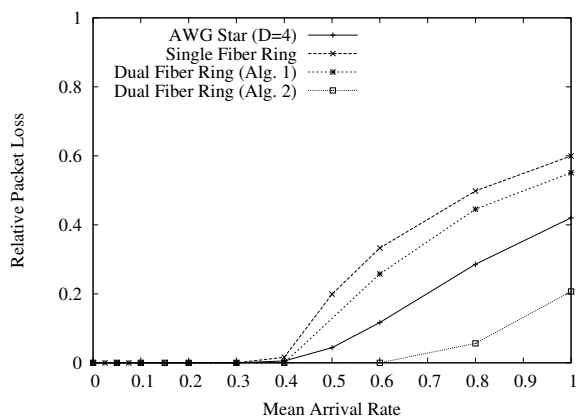


Fig. 10. Relative packet loss for uniform Bernoulli traffic without fairness control, $N = 32$

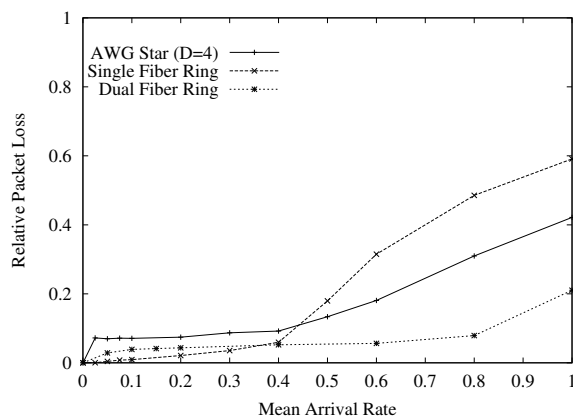


Fig. 11. Relative packet loss for uniform self-similar traffic without fairness control, $N = 32$

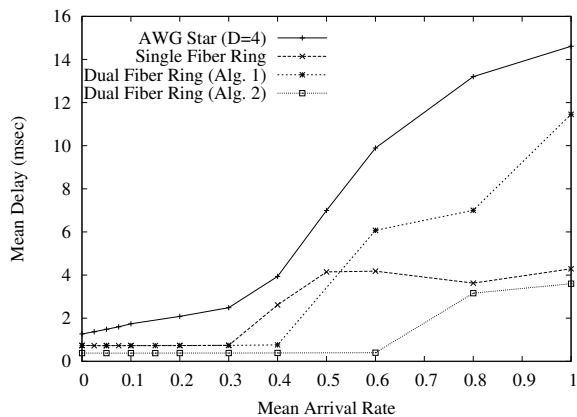


Fig. 12. Mean delay for uniform Bernoulli traffic without fairness control, $N = 32$

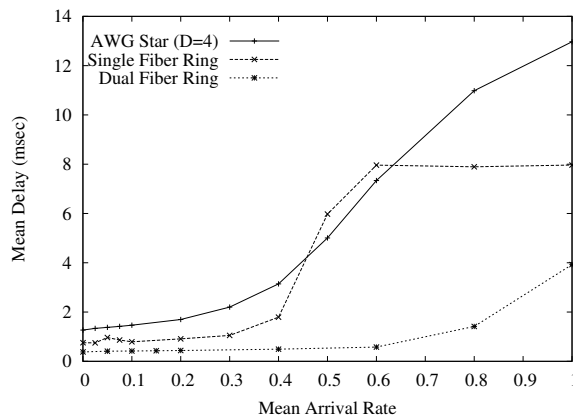


Fig. 13. Mean delay for uniform self-similar traffic without fairness control, $N = 32$

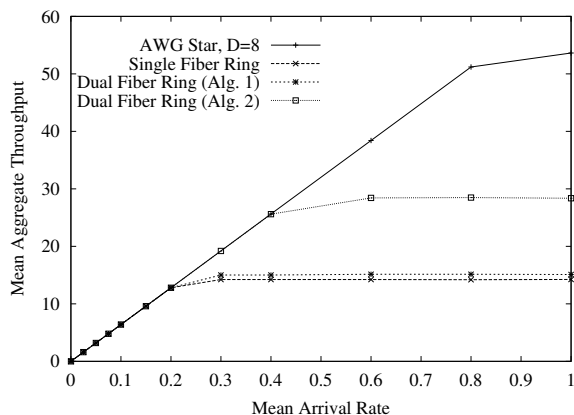


Fig. 14. Mean aggregate throughput for uniform Bernoulli traffic without fairness control, $N = 64$

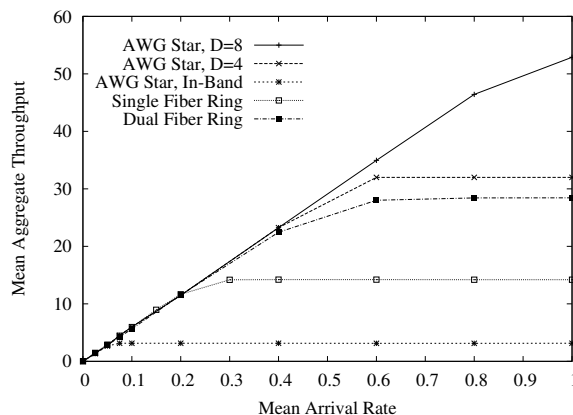


Fig. 15. Mean aggregate throughput for uniform self-similar traffic without fairness control, $N = 64$

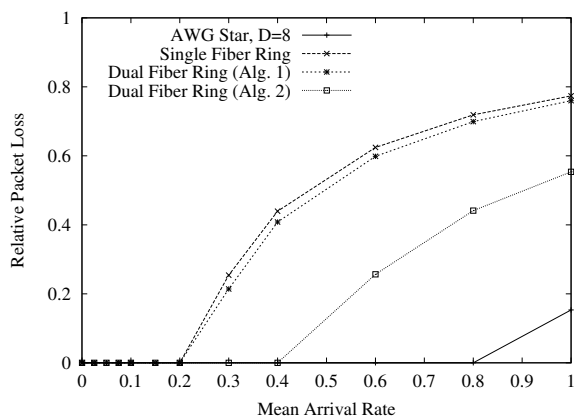


Fig. 16. Relative packet loss for uniform Bernoulli traffic without fairness control, $N = 64$

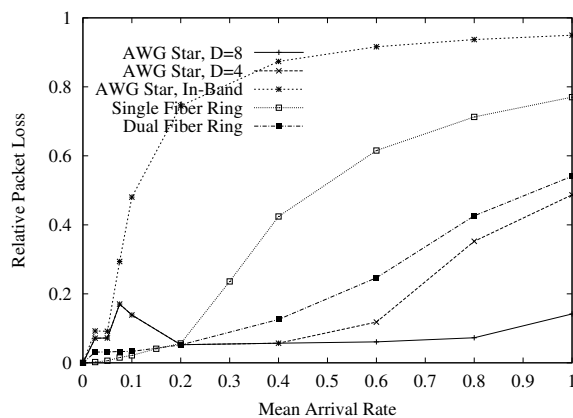


Fig. 17. Relative packet loss for uniform self-similar traffic without fairness control, $N = 64$

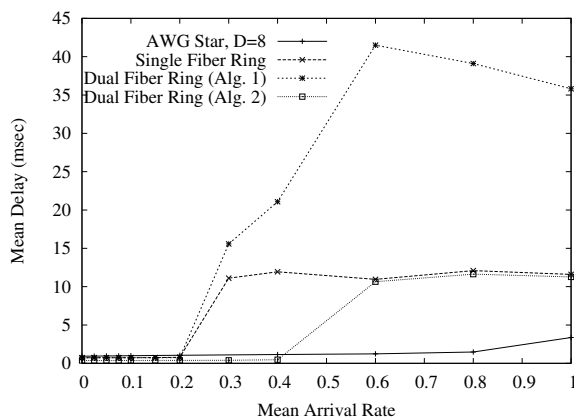


Fig. 18. Mean delay for uniform Bernoulli traffic without fairness control, $N = 64$

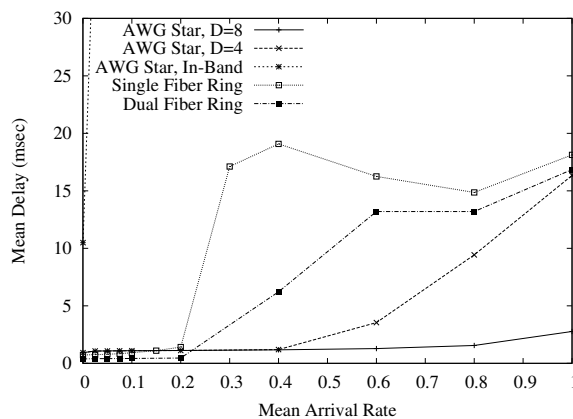


Fig. 19. Mean delay for uniform self-similar traffic without fairness control, $N = 64$

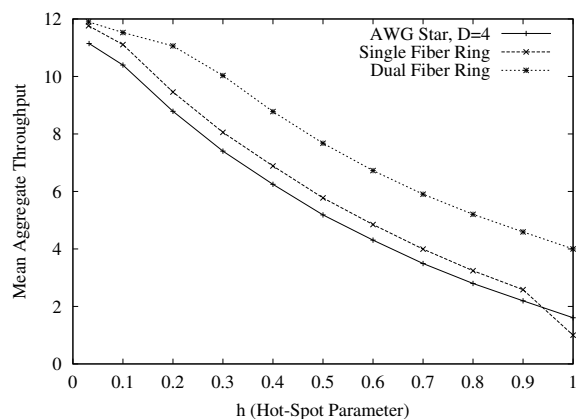


Fig. 20. Mean aggregate throughput as a function of the fraction of hot-spot traffic h with $N = 32$ and $\sigma = 0.4$, fixed without fairness control

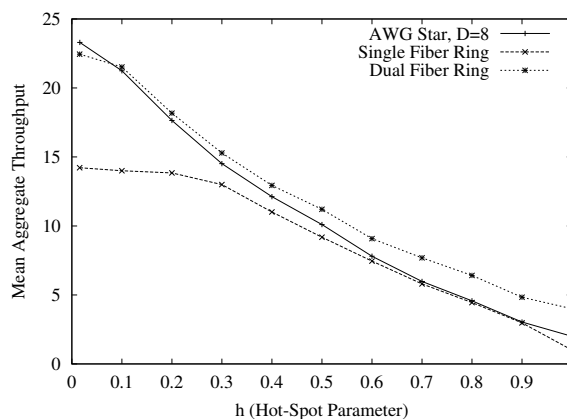


Fig. 21. Mean aggregate throughput as a function of the fraction of hot-spot traffic h with $N = 64$ and $\sigma = 0.4$, fixed without fairness control

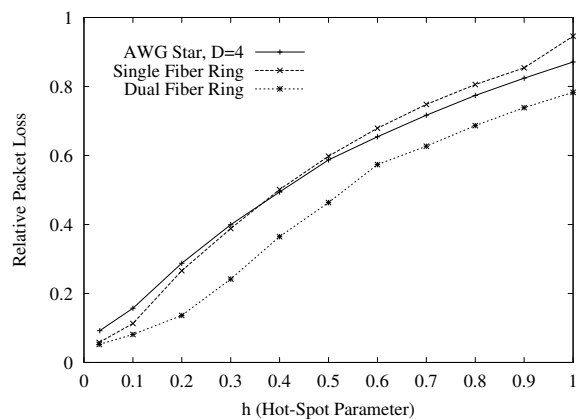


Fig. 22. Relative packet loss as a function of the fraction of hot-spot traffic h with $N = 32$ and $\sigma = 0.4$, fixed without fairness control

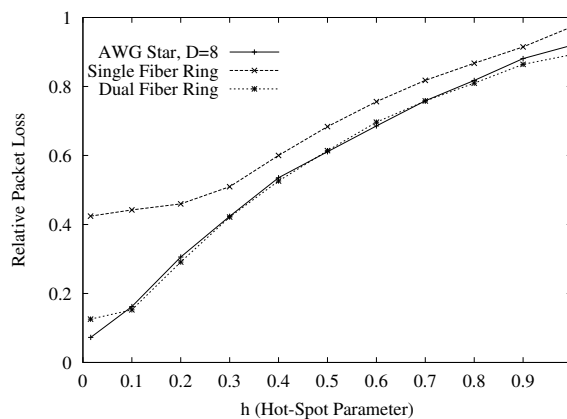


Fig. 23. Relative packet loss as a function of the fraction of hot-spot traffic h with $N = 64$ and $\sigma = 0.4$, fixed without fairness control

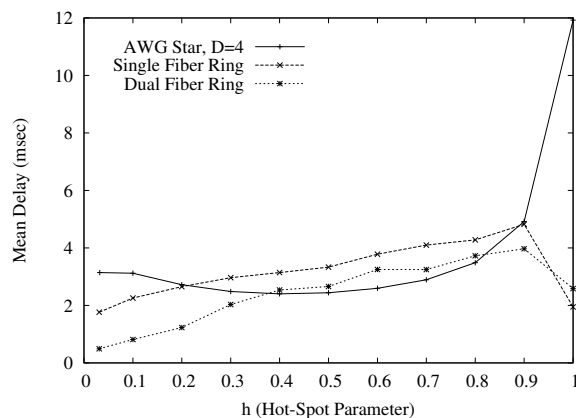


Fig. 24. Mean delay as a function of the fraction of hot-spot traffic h with $N = 32$ and $\sigma = 0.4$, fixed without fairness control

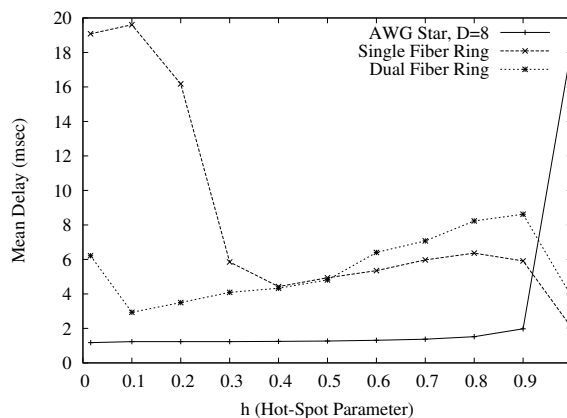


Fig. 25. Mean delay as a function of the fraction of hot-spot traffic h with $N = 64$ and $\sigma = 0.4$, fixed without fairness control

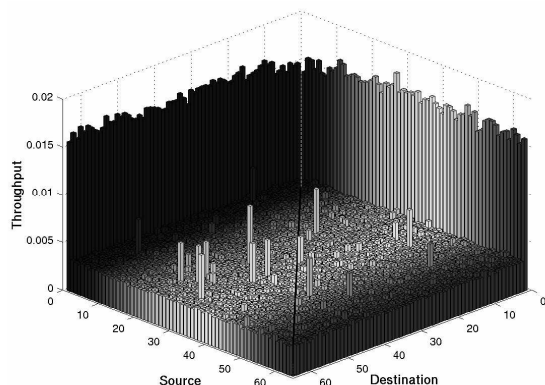


Fig. 26. Pairwise mean aggregate throughput of AWG star network for self-similar hot-spot traffic scenario, $\sigma = 0.4$ and $h = 0.3$

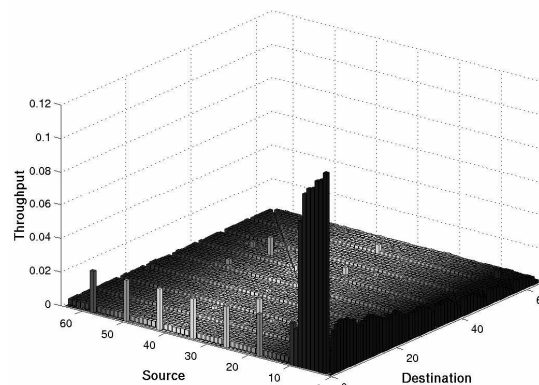


Fig. 27. Pairwise mean aggregate throughput of single-fiber ring network for self-similar hot-spot traffic scenario, $\sigma = 0.4$ and $h = 0.3$

other destinations [15]. Spatial reuse may cause *starvation*, which occurs when a node is constantly being covered by up-stream ring traffic and thus is not able to access the ring for very long periods of time [43]. This fairness problem has received considerable attention in the literature [9], [15], [17], [44], [45].

In this comparative study, for both single-fiber and dual-fiber ring networks we use the fairness control described in [17] which is a modified form of ATMR [45]. (We note that a modified fairness control of DQDB (Distributed Queue Dual Bus) called DQBR (Distributed Queue Bi-directional Ring) was proposed in [9] for dual-fiber ring networks. However, the DQBR scheme can not be directly employed in the considered network which uses destination stripping with spatial wavelength reuse and $N > \Lambda$.) The used fairness control represents a credit allocation scheme and provides fair channel access by means of a distributed credit mechanism and a cyclic reset scheme based on a monitoring approach. The fairness control algorithm works as follows. Initially, each node is allocated a predefined credit, referred to as *window size* W , and is set to the active state. The node status (active or inactive) for a channel is included in a so-called *busy address field* of the SCM header in case of the single-fiber ring and on the control channel in case of the dual-fiber ring network. Each node decreases the window size whenever it uses a free slot to send a packet. If the node is still in the active state, i.e., if the window size is larger than zero, the node sets the busy address field to the node's address. When the window size reaches zero, the node changes its state to the inactive state, i.e., the node is not allowed to send any data using the wavelength and leaves the busy address field unchanged. Thus, all nodes in the network can see which nodes are in the active state. If a node receives a slot with busy address field set to the node itself, the node knows that all other nodes are in the inactive state. The node then immediately sends a reset message to all other nodes by setting the *reset-request field* in the SCM header or in the control channel and resets its window size to the predefined window size W . The node sends the reset message only once and waits for the reset message to circulate around the entire ring network. When the reset message is received by the node which sent the reset message, the message is stripped from the ring. When a node receives a reset-request, the node sets its status to the active state, sets the window size for the channel to the predefined window

size W and forwards the reset-request. This algorithm is invoked on all Λ channels at each node.

The window size W specifies the credit/quota of usable slots and determines the duration of the activity cycles. Thus, W represents the main parameter of the fairness control. Figs. 28 and 29 depict the throughput-delay performance of the single-fiber ring network for uniform Bernoulli traffic and different window size $W = \{20, 50, 100\}$, where the number of nodes in the network is fixed of 32, $N = 32$, whereas Figs. 30 and 31 depict the throughput-delay performance of the single-fiber ring network for uniform self-similar traffic and different window size $W = \{50, 300, 500, 700, 1000\}$ with and without fairness control, where the number of nodes in the network is fixed of 64, $N = 64$.

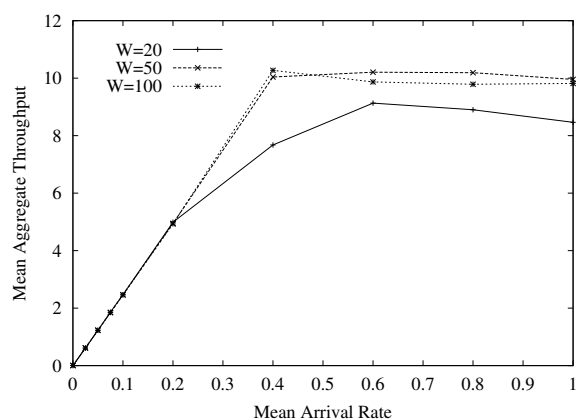


Fig. 28. Throughput of TT-FR ring network for uniform Bernoulli traffic with $W = \{20, 50, 100\}$ and $N = 32$

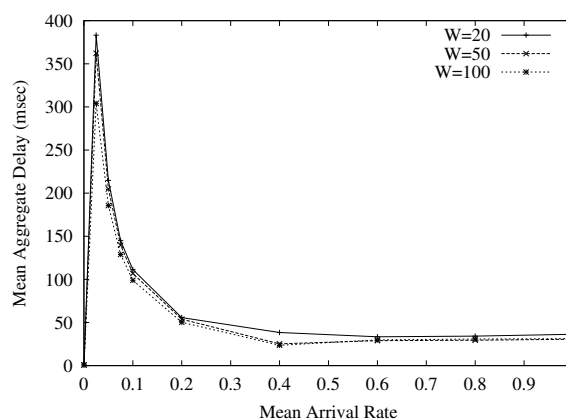


Fig. 29. Mean delay of TT-FR ring network for uniform Bernoulli traffic with $W = \{20, 50, 100\}$ and $N = 32$

Fig. 30 shows the mean aggregate throughput vs. mean arrival rate. We observe and re-confirm the well-known trade-off between (throughput) fairness and aggregate network performance, i.e., fairness control degrades the aggregate (throughput) performance of the network (this holds also for the mean delay, as shown in Fig. 31). We observe from Fig. 30 that a medium window size $W \in \{300, 500\}$ achieves the largest mean aggregate throughput. Whereas choosing a small or large W leads to a decreased mean aggregate throughput. For a small window size ($W = 50$) each node is allowed to access the channels for a limited period of time. After using its quota a node has to stop transmitting and wait for other nodes' transmission, even though they may not have packets to send, resulting in a decreased throughput. On the other hand, for a large window size $W \in \{700, 1000\}$ nodes tend to prevent each other from transmission since nodes having used their quota have to wait for the other nodes' transmission for a longer period of time on average. As a result, nodes are idle for a longer period of time resulting in a smaller mean aggregate throughput. Note that this holds in particular at small to medium traffic loads. At heavy traffic (large mean arrival rate) each node has enough data packets to send such that nodes do not prevent each other from transmission.

Fig. 31 depicts the mean delay vs. mean arrival rate. Again, we see the trade-off between fairness and overall performance. While at medium to high traffic loads the mean delay gradually increases with an increasing mean arrival rate, we observe some counterintuitive results at small arrival rates. The mean delay

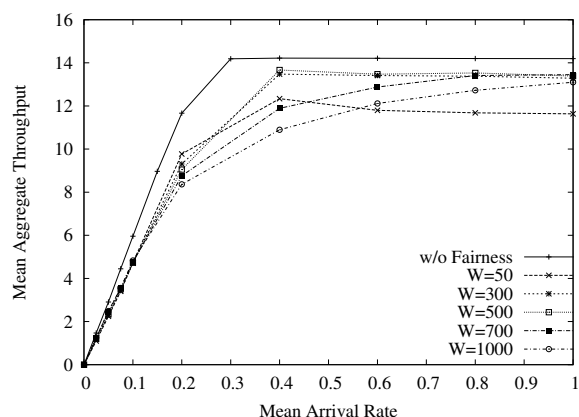


Fig. 30. Mean aggregate throughput of single-fiber ring network for uniform self-similar traffic with $W = \{50, 300, 500, 700, 1000\}$ and $N = 64$.

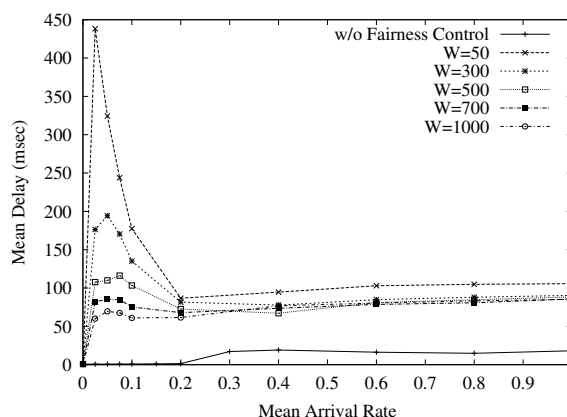


Fig. 31. Mean delay of single-fiber ring network for uniform self-similar traffic with $W = \{50, 300, 500, 700, 1000\}$ and $N = 64$.

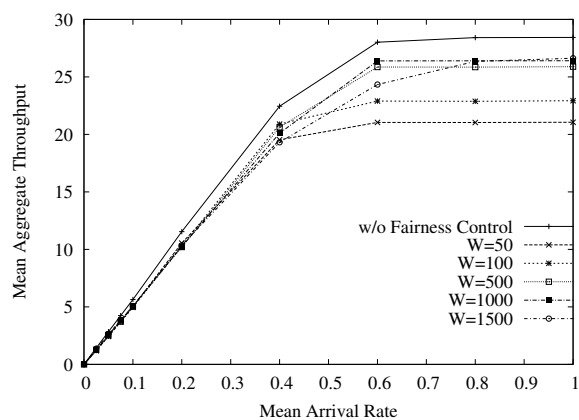


Fig. 32. Mean aggregate throughput of dual-fiber ring network for uniform self-similar traffic with $W = \{50, 100, 500, 1000, 1500\}$ and $N = 64$.

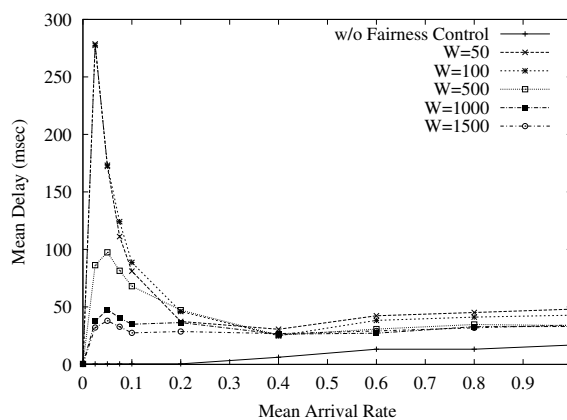


Fig. 33. Mean delay of dual-fiber ring network for uniform self-similar traffic with $W = \{50, 100, 500, 1000, 1500\}$ and $N = 64$.

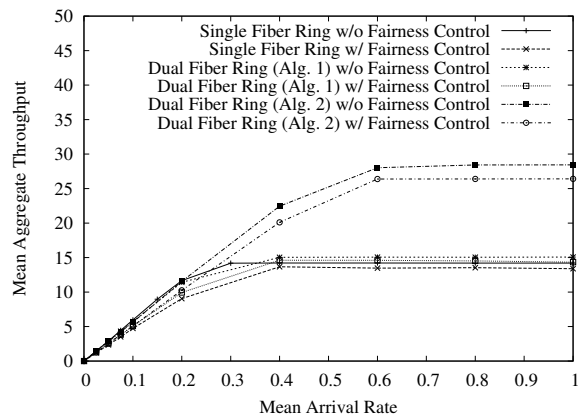


Fig. 34. Mean aggregate throughput of ring networks for uniform self-similar traffic.

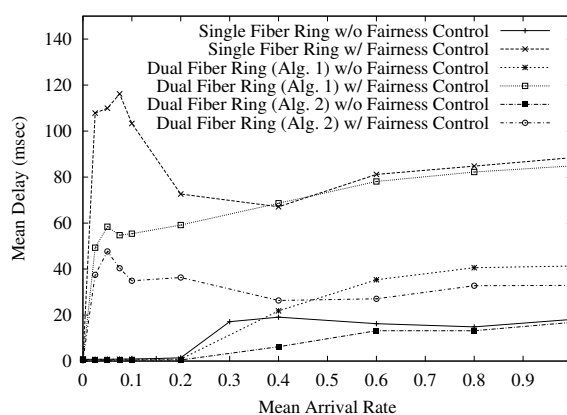


Fig. 35. Mean delay of ring networks for uniform self-similar traffic.

is significantly larger at small arrival rates, especially for small window size W . This is due to the fact that with smaller W nodes' transmission activities are interrupted more often. To resume transmission, an interrupted node has to wait for the remaining nodes to use up their quota which takes longer for smaller mean arrival rates due to the lack of generated traffic. As a result, the mean delay is rather large at light traffic and decreases with increasing amount of generated traffic, i.e., mean arrival rate. By considering the results shown in Figs. 30 and 31, we conclude that we can get optimal performances with window size $W = 500$ for single-fiber ring.

Performances relation with different window size are also measured in dual-fiber ring network as shown in Figs. 32 and 33. Similar observations with single-fiber ring are made in dual-fiber ring network. Optimal performance can be obtained with window size $W = 1000$ for dual-fiber ring network. Performance comparison of single-fiber ring and dual-fiber ring (Alg. 1 as well as Alg. 2) without and with fairness control are depicted in Figs. 34 and 35 for uniform self-similar traffic with window size for $W = 500$ for single-fiber ring and $W = 1000$ for dual-fiber ring and the number of nodes in the network is set to 64, $N = 64$. From the observation made in this section, we use fairness window size of $W = 500$ for single-fiber ring and $W = 1000$ for dual-fiber ring network for the following results.

E. Uniform (Balanced) Traffic Scenario with Fairness Control

Performance of the ring with fairness control and star network for uniform (balanced) traffic are presented in this section. The nodes in the single-fiber ring networks deploy the ATMR fairness control with a window size of $W = 500$, while ATMR fairness control with a window size of $W = 1000$ is used in the dual-fiber ring network as described in previous section. We consider both Bernoulli and self-similar traffic. The results are shown in Figs. 36 – 41 for $N = 32$ and Figs. 42 – 47 for $N = 64$ for both Bernoulli and self-similar traffic. As described in preceding section, we use IB signaling for $N = 32$ and OB signaling for $N = 64$ in star network. Both OB and IB signaling are used in self-similar traffic as shown in Figs. 43, 45, and 47.

Clearly, in the single-hop star network the mean hop distance is minimum (unity). The degree of spatial wavelength reuse is controlled by the AWG degree D since all Λ wavelengths can be used at each port simultaneously, as illustrated in Fig. 5. Therefore, the star network with $D = 8$, $S = 8$, and $R = 1$ is able to achieve about twice the throughput of the setup with $D = 4$, $S = 16$, and $R = 2$ which is also reflected by the results of the simulation in Fig. 43. Note that for full connectivity the maximum AWG degree is limited by $D \leq \Lambda$, resulting in an upper bound on the spatial wavelength reuse. Moreover, to fully exploit the capacity of the AWG at least $S \geq \Lambda$ nodes have to be attached to each port (cf. Figs. 4 and 5). When comparing the out-of-band signaling with the inband signaling approach it turns out that the latter one severely limits the performance of the star network. The capacity of the inband channel does not suffice to (re)transmit all control packets leading to a much smaller throughput and to a significantly increased delay as shown in Figs. 43 and 47 (the delay with inband signaling quickly shoots up and levels out around 380 msec, which extends beyond the delay range shown in Fig. 47). In contrast, the external

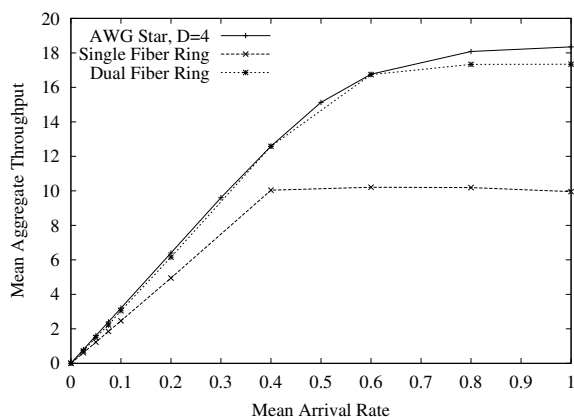


Fig. 36. Mean aggregate throughput for uniform Bernoulli traffic with fairness control, $N = 32$.

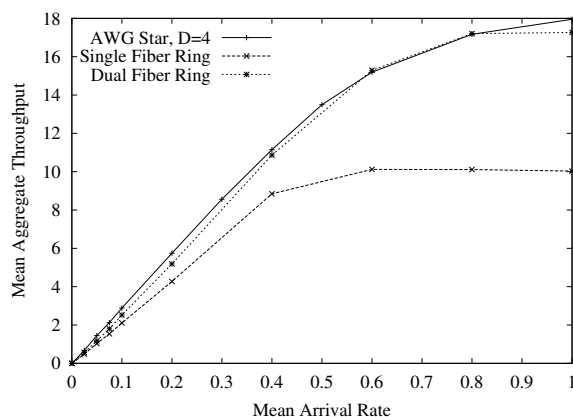


Fig. 37. Mean aggregate throughput for uniform self-similar traffic with fairness control, $N = 32$.

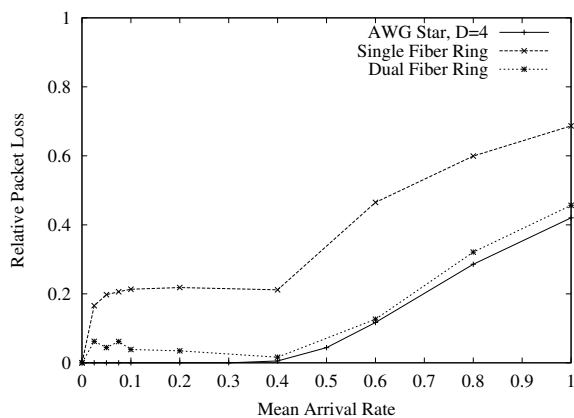


Fig. 38. Relative packet loss for uniform Bernoulli traffic with fairness control, $N = 32$.

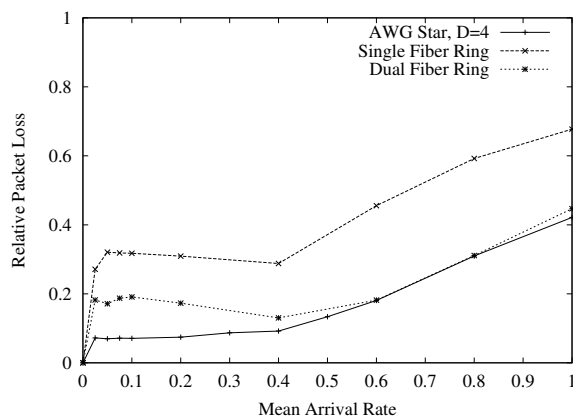


Fig. 39. Relative packet loss for uniform self-similar traffic with fairness control, $N = 32$.

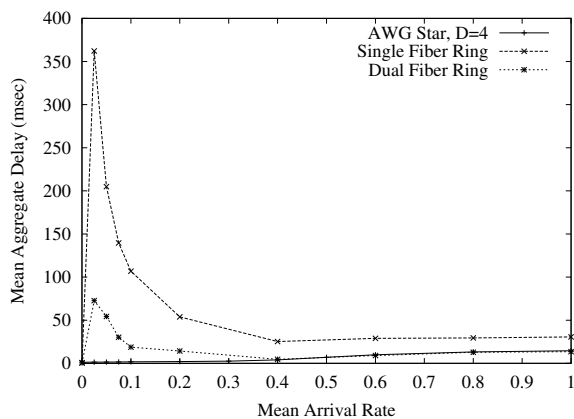


Fig. 40. Mean delay for uniform Bernoulli traffic with fairness control, $N = 32$.

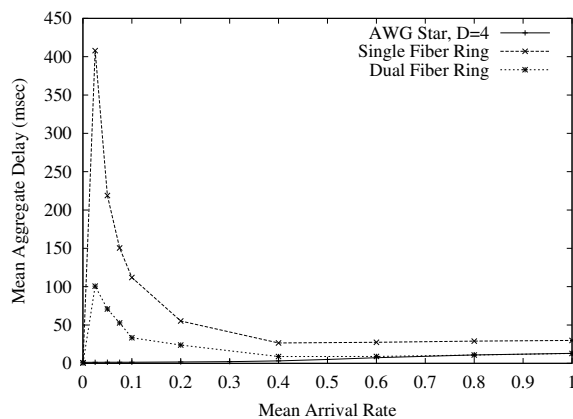


Fig. 41. Mean delay for uniform self-similar traffic with fairness control, $N = 32$.

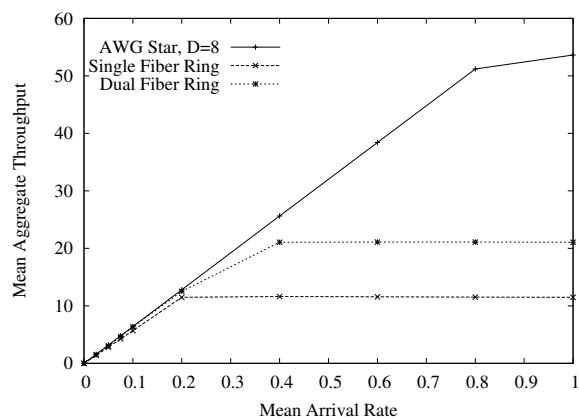


Fig. 42. Mean aggregate throughput of star and ring networks for uniform Bernoulli traffic, $N = 64$.

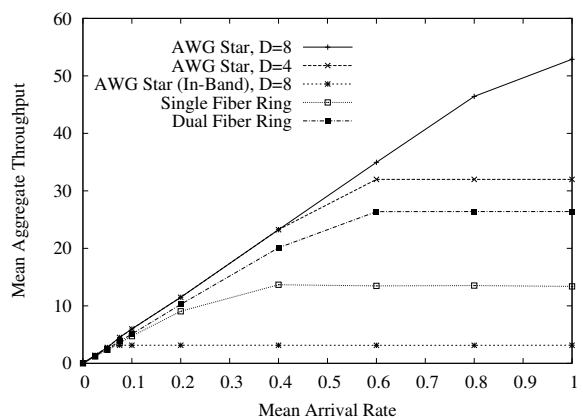


Fig. 43. Mean aggregate throughput of star and ring networks for uniform self-similar traffic, $N = 64$.

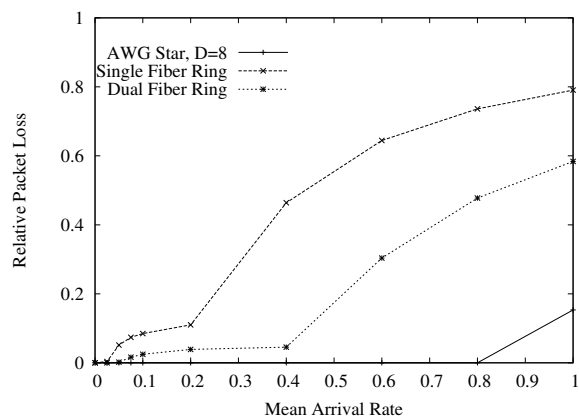


Fig. 44. Relative packet loss of star and ring networks for uniform Bernoulli traffic, $N = 64$.

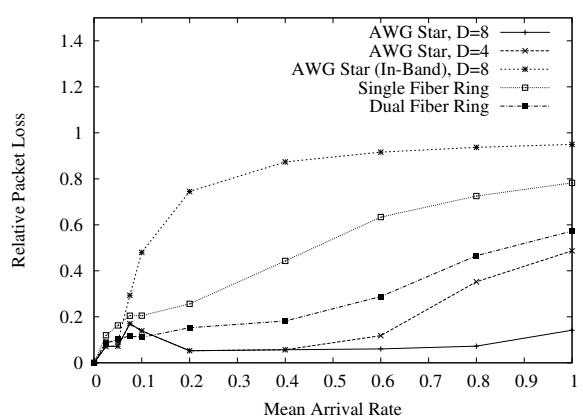


Fig. 45. Relative packet loss of star and ring networks for uniform self-similar traffic, $N = 64$.

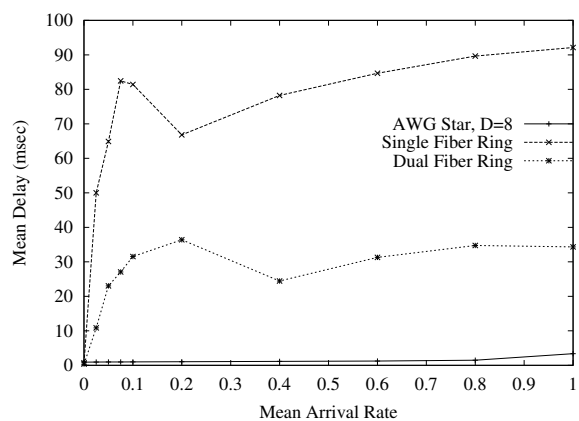


Fig. 46. Mean delay of star and ring networks for uniform Bernoulli traffic, $N = 64$.

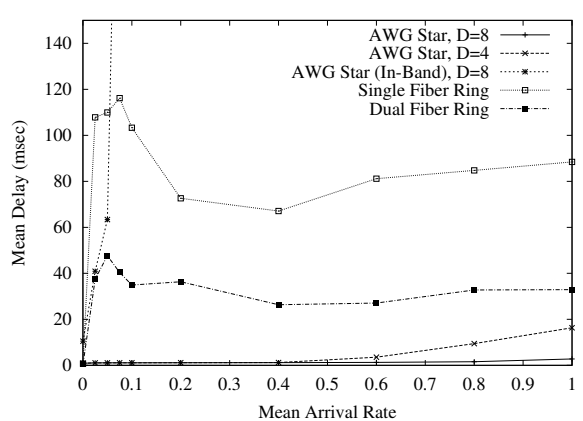


Fig. 47. Mean delay of star and ring networks for uniform self-similar traffic, $N = 64$.

control channel provides sufficient capacity, leading to only few collisions and to aggregates consisting mostly of only a single packet. In the following sections only the star with external control channel based on an AWG of degree $D = 8$ is considered for $N = 64$.

When comparing the results of the star with those of the ring in Figs. 36 – 47 the latter one is clearly outperformed in terms of all measured performance metrics. The difference in the throughput of the networks, shown in Figs. 42 and 43, reflect the theoretical capacity limits of $2 \cdot \Lambda = 16$ in the single fiber ring, $4 \cdot \Lambda = 32$ in the bidirectional ring, and $D \cdot \Lambda = 64$ in the star. In the star, up to about $\sigma = 0.8$ nearly all packets are scheduled by the first control packet leading to a small delay, depicted in Figs. 46 and 47, which is close to the theoretical minimum of two times the propagation delay of the ring diameter and nearly no packet is lost. The packet loss shown in Figs. 44 and 45 also illustrates the difference between Bernoulli and self-similar traffic. The latter one is bursty and leads to VOQ overflows even if the network is principally able to handle the offered amount of traffic and the VOQs are relatively short. As the networks saturate the difference between the two traffic models vanishes. Note from Figs. 42 and 43 that the throughput of the ring network for self-similar traffic is slightly larger than for Bernoulli traffic. However, the throughput of the ring network for Bernoulli traffic without fairness control is slightly larger than for self-similar traffic as shown in Figs. 14 and 15. The larger throughput for self-similar traffic with fairness control is due to the window based nature of fairness control. As described in Section IV-D the node which sends all its quota has to wait until the other nodes finish using their quota. The bursty nature of the self-similar traffic helps in finishing the nodes' quota. Thus, the ring networks with fairness control tend to have larger throughput for self-similar traffic. In the following we only consider the more realistic self-similar traffic model.

F. Non-uniform (Unbalanced) Traffic Scenario with Fairness Control

We present the performance of ring network with fairness control and star network for self-similar traffic. In the ring networks the ATMR fairness control is employed with window size of $W = 500$ for single-fiber and $W = 1000$ for dual-fiber ring network as discussed above.

The performance results are shown in Figs. 48, 50, and 52 for $N = 32$, and Figs. 49, 51, and 53 for $N = 64$. As h increases the throughput steadily decreases. For $h = 1$, the throughput of the star network is roughly equal to two, which corresponds to the one transmitter plus one receiver in the hot-spot. The throughput in the ring networks for $h = 1$ is only roughly half the combined number of transmitters and receivers in the hot-spot (two in single-fiber ring network and four in dual-fiber ring network). This is due to a degeneration of the ATMR fairness control for $h = 1$ which can be overcome by a modified fairness control as described more detail later in this section. Interestingly, we observe that for moderate h values in the range from approximately 0.5 to 0.8, the throughput in the single-fiber ring network is relatively close to the throughput in the dual-fiber network. We also observe that with an increasing fraction h of hotspot traffic, the relative packet loss increases steadily. This is mainly due to the limited capacity of the hot-spot's transceiver(s), which results in most of the packets destined to or originating from the server

to be lost.

We observe from Fig. 53 that there are marked differences in the delay. In the star, the data aggregates corresponding to hot-spot traffic are mostly of the maximum size and experience a large delay. However, the client-to-client traffic is still transported efficiently via numerous data aggregates, mostly of the minimum size. Therefore, the delay does not increase significantly until there is rarely any more client-to-client communication. In the ring, client-to-client traffic, except that on the hot-spot's home channel, does not experience an increased delay. In contrast, any packet transmitted on the congested home channel of the hot-spot and packets originating from the hot-spot (transmitter bottleneck) are additionally delayed. Therefore, as the fraction of hot-spot traffic increases the delay also increases. Note that for $h = 1.0$, the delay in the ring networks is smaller than in the case of uniform traffic (Fig. 47), which is due to the degeneration of the ATMR fairness control for $h = 1$.

Basic idea behind the ATMR fairness control algorithm is credit allocation. Every node has the same number of credit to use free slot. In special case, $h = 1$, client nodes use only one wavelength, i.e., drop wavelength of the server node. Thus, credits for other wavelength are never expired. When the server node uses up the credit for the wavelengths other than the drop wavelength of the node itself, the node cannot send any data and waits for reset message which is never generated. Thus, there is no data in wavelength other than the server node's drop wavelength after the window of the server node expires. All nodes (including server nodes) use only wavelength which is the server's drop wavelength. Thus most of the packets destined to or originating from the server are lost, because of the limited capacity of the hot-spot's transceiver(s). Fairness controls proposed so far in the literatures are, generally, credit allocation based algorithms [9], [15], [17], [44], [45]. Thus if the traffic pattern is not uniform, the network will suffer serious bottleneck and cannot balance the network which causes another fairness problem. One possible solution for the special case, $h = 1$, is to use fairness control only in the server's drop wavelength and not to use fairness control in other wavelengths. Only server node uses the wavelengths other than the server node's drop wavelength, no fairness control is needed for the wavelengths. Using this modified algorithm, we get aggregate throughput of 1.96, relative packet loss of 0.921, and mean delay of 17.02 msec for single-fiber ring. For dual-fiber ring, we get aggregate throughput of 3.87, relative packet loss of 0.9, and mean delay of 10 msec. By using this simple modified algorithm, throughput increases and delay decreases. Thus more attention should be paid on the fairness control issues especially on unbalanced traffic pattern. In terms of delay, the star and the ring perform differently.

The source-destination pairwise metrics in the single-fiber ring network with fairness control are shown in Figs. 54 and 55 for the aggregate throughput and the relative packet loss probability, respectively. Compared to Fig. 27, the applied fairness control scheme balances the network.

G. Multicast Traffic

In this section we compare the performance of the ring and star WDM networks for multicast (multi-destination) traffic. Multicast traffic is expected to account for a significant portion of the traffic in future

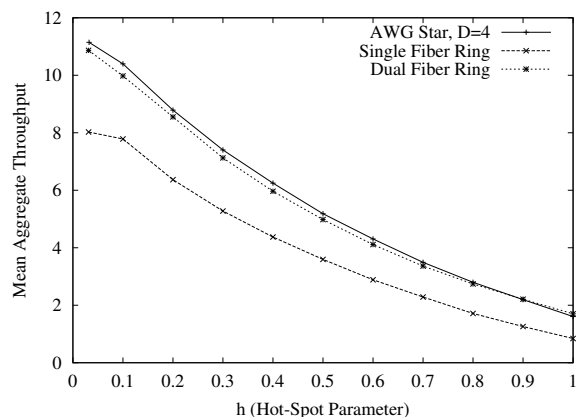


Fig. 48. Mean aggregate throughput as a function of the fraction of hot-spot traffic h with $N = 32$ and $\sigma = 0.4$, fixed

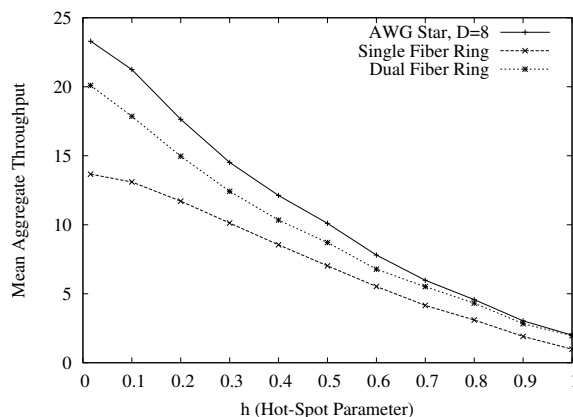


Fig. 49. Mean aggregate throughput as a function of the fraction of hot-spot traffic h with $N = 64$ and $\sigma = 0.4$, fixed

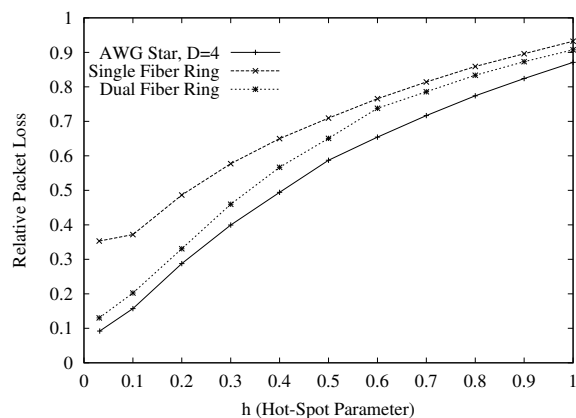


Fig. 50. Relative packet loss as a function of the fraction of hot-spot traffic h with $N = 32$ and $\sigma = 0.4$, fixed

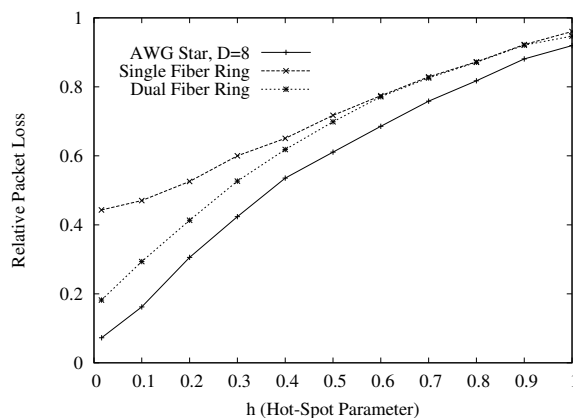


Fig. 51. Relative packet loss as a function of the fraction of hot-spot traffic h with $N = 64$ and $\sigma = 0.4$, fixed

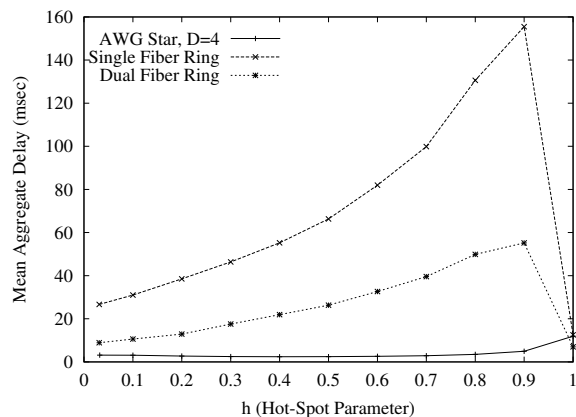


Fig. 52. Mean delay as a function of the fraction of hot-spot traffic h with $N = 32$ and $\sigma = 0.4$, fixed

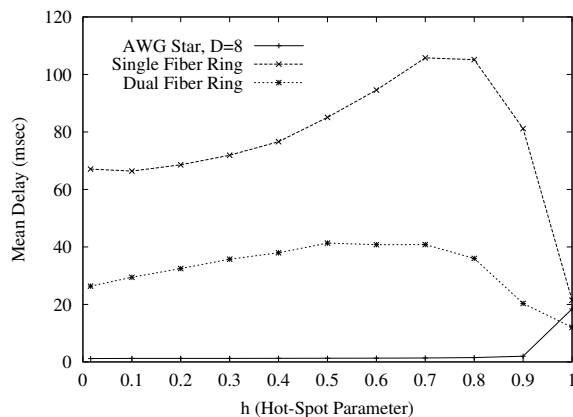


Fig. 53. Mean delay as a function of the fraction of hot-spot traffic h with $N = 64$ and $\sigma = 0.4$, fixed

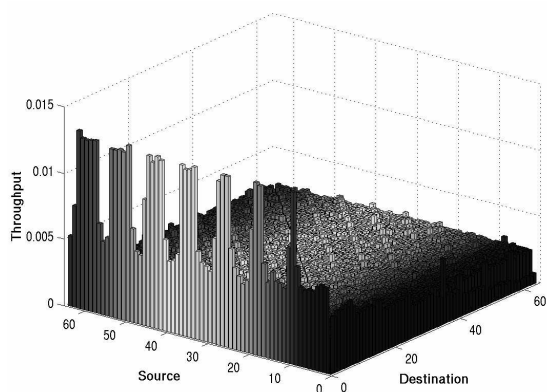


Fig. 54. Pairwise mean aggregate throughput of single-fiber ring network with fairness control for self-similar hot-spot traffic with $\sigma = 0.4$ and $h = 0.3$

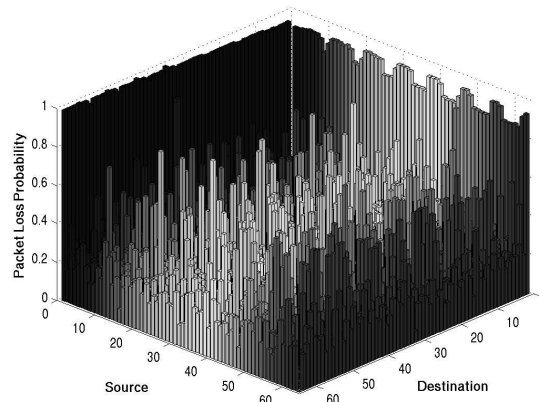


Fig. 55. Pairwise packet loss probability of single-fiber ring network with fairness control for self-similar hot-spot traffic with $\sigma = 0.4$ and $h = 0.3$

metro WDM networks due to applications such as video conferencing, tele-medicine, distributed games, and content distribution. Multicasting in ring network has received relatively little attention [12], [46], similarly, multicasting in the AWG based metro WDM network has received only limited attention so far [47]. In this section we first outline the modifications to the node architectures and MAC protocols in the ring and star network to accommodate a mix of multicast and unicast traffic. We then define the considered performance metrics for this traffic mix and present the results of our comparisons.

In both the single-fiber ring and the star network, each node is equipped with Λ buffers (each of capacity B packets) for multicast traffic (in the dual-fiber network each node has $\Lambda/2$ multicast buffers), in addition to the $N - 1$ buffers (each of capacity B packets) for unicast traffic. The multicast buffers are operated as follows. First recall that in the single-fiber ring network each wavelength is the home channel for N/Λ nodes (in the dual-fiber ring network each wavelength on a given fiber is the home channel of $2 \cdot N/\Lambda$ nodes). Thus a packet transmission on a given wavelength can reach up to N/Λ destination nodes of a multicast in the single-fiber ring network (or up to $2 \cdot N/\Lambda$ nodes in the dual-fiber network). Now, one of the Λ multicast buffers is assigned to each of the Λ wavelengths in the single-fiber ring network. (In the dual-fiber ring network one multicast buffer is assigned to each of the $\Lambda/2$ home channels.) The destination nodes of a given multicast are partitioned into up to Λ groups in the single-fiber ring (up to $\Lambda/2$ groups in the dual-fiber ring) according to the different home channels of the destination nodes. A copy of the multicast packet is generated for each group of destination nodes and placed in the corresponding multicast buffer. If all nodes of a given multicast share the same home channel, then only one packet copy is generated and placed in the corresponding multicast buffer. If a multicast has destination nodes on each of the home channels, then Λ packet copies are generated, and one each is placed in the Λ multicast buffers in the single-fiber network (in the dual-fiber network $\Lambda/2$ copies are generated and placed). In the star network one of the Λ multicast buffers in a given node is assigned to each of the Λ wavelengths or equivalently the $\Lambda = D$ destination splitters (for the considered scenario

with $R = 1$, generally, if $R \geq 1$ then R multicast buffers would be assigned to each destination splitter). The destination nodes of a multicast are partitioned according to the splitters that the destination nodes are attached to. If all destination nodes are attached to the same splitter, then one packet copy is placed in the corresponding multicast buffer. If a multicast has destinations at all splitters, then Λ packet copies are generated and one each is placed in the Λ multicast buffers.

The MAC protocol for multicast packet (copies) in ring networks works as follows. The addresses of the intended destination nodes of a given multicast packet copy on a given home channel are included in the control information corresponding to the packet. Each node monitors its home channel as described in Section II-B. When a node receives a data packet, it checks whether there are additional destinations downstream. If so, the node forwards the packet to the downstream nodes. If the node is the last destination, then it takes the packet off the ring. To keep the delays small for multicasts, which inherently use the bandwidth more efficiently than unicasts, we send the multicast packet copies using Alg. 1 (see Section IV-E) in the direction that has the first vacant slot.

We employ the Longest Queue (LQ) buffer selection in both ring and star network. We count one for a unicast packet. For a given multicast packet copy we count the number of intended destination nodes that it will reach, i.e., up to N/Λ on the single-fiber ring and star networks, and up to $2 \cdot N/\Lambda$ on the dual-fiber ring network. This counting scheme tends to give a multicast packet copy higher priority according to the number of destination that it reaches.

In the star network, multicast packet copies are not combined into aggregates and the scheduler schedules a multicast packet copy transmission only if all intended destination nodes at the respective splitter are free.

In the performance evaluation for mixed unicast and multicast traffic, we consider the following performance metrics.

- The mean aggregate receiver throughput is defined as the number of receivers that are receiving a packet destined to them in steady state.
- The mean aggregate transmitter throughput is defined as for unicast traffic in Section IV-A.
- The mean aggregate multicast throughput is defined as the mean number of multicast completions per slot. The multicast throughput is equal to the ratio of the mean transmitter throughput to the mean number of packet copy transmissions required to reach all intended destination nodes of a given multicast packet. The multicast throughput thus measures the multicast efficiency of each packet copy transmission.
- The mean packet delay is defined similar to the unicast traffic scenario in Section IV-A. For a multicast packet, however, we consider the individual delays until the complete reception of the packet by the individual receivers. The individual delays experienced until a given multicast packet is received by its destination nodes are all individually counted when evaluating the mean packet delay.
- The relative packet loss is defined as for unicast traffic, with the differences that (i) a generated

multicast packet with m destination nodes counts as m generated packets, and (ii) a multicast packet copy destined to n destination nodes that finds its multicast buffer full and is dropped counts as n dropped packets.

In our simulations for mixed unicast and multicast traffic we consider uniform self-similar traffic with a fraction p_m of multicast traffic. More specifically, each node generates new packets as in the case of unicast traffic. With probability p_m a given newly generated packet becomes a multicast packet. For a given multicast packet the number of destination nodes is drawn independently randomly from a uniform distribution over $[1, N - 1]$, and the destination nodes are distributed uniformly randomly over the other $N - 1$ nodes.

For the simulations reported here the fraction of multicast traffic is set to $p_m = 0.3$. The window size for fairness control is set as for unicast traffic to $W = 500$ in the single-fiber network and $W = 1000$ for the dual-fiber network. Figs. 56, 57, and 58 give the mean aggregate receiver, transmitter, and multicast throughput as a function of the mean arrival rate σ . A number of observations are in order. First, we observe that the dual-fiber ring network achieves close to twice the receiver throughput of the single-fiber ring. This is because a packet copy transmitted on a given wavelength in the dual-fiber ring network can reach up to twice the number of nodes compared to a packet copy transmitted on the single-fiber ring. Hence the difference in receiver throughput between single-fiber and dual-fiber ring despite both having roughly the same transmitter throughput and multicast throughput. We also observe that in both ring networks the transmitter throughput and multicast throughput have a slight peak around $\sigma = 0.2$ and then level off as the traffic load is increased further. At the same time the receiver throughput continues to increase. This is because the LQ buffer selection policy tends to give priority to multicast packets, especially at increasing network loads when the buffers tend to get filled (and packet loss becomes large, see Fig. 59). To see this, recall that we count the number of destination nodes of the multicast packet copies in the LQ buffer selection, as is natural and reasonable. In the single-fiber ring network each multicast packet copy is destined on average to $N/(2 \cdot \Lambda) = 4$ destination nodes ($2 \cdot N/(2 \cdot \Lambda) = 8$ in the dual-fiber network). Thus a unicast packet buffer completely filled with B packets has about the same priority in the buffer selection as a multicast buffer filled to a quarter of its capacity in the single-fiber network (one eighth in the dual-fiber network). As the multicast buffers are filled up to higher levels they are given priority over unicast packet buffers. More specifically, priority is given to the multicast buffer holding the packet copies with the largest number of destinations.

For the star network, on the other hand, we observe that transmitter and receiver throughput as well as multicast throughput continue to increase as the traffic load increases. The receiver throughput, however, stays well below the levels reached by the dual-fiber ring. This is due to the combined dynamics of buffer selection and data packet scheduling in the star network. Similar to the ring network, the multicast packet copies are given priority in the LQ selection of the VOQs for which control packets are sent. The multicast data packet copies, however, are more difficult to schedule than unicast packets, as the copies require all

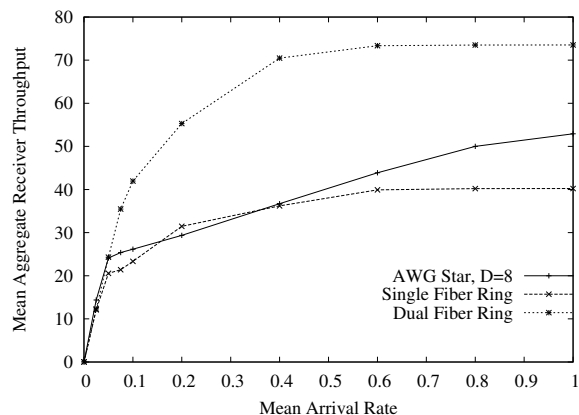


Fig. 56. Aggregate receiver throughput for uniform self-similar traffic with $p_m = 30\%$ multicast traffic

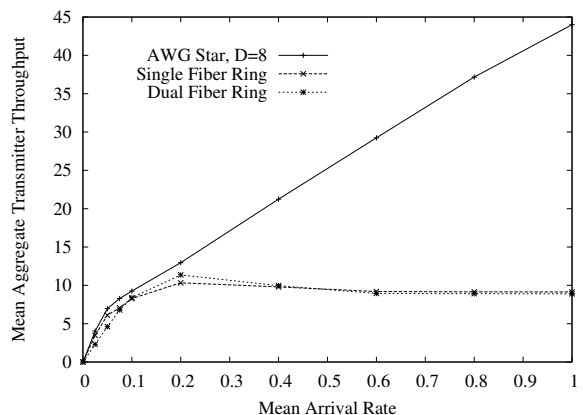


Fig. 57. Aggregate transmitter throughput for uniform self-similar traffic with $p_m = 30\%$ multicast traffic

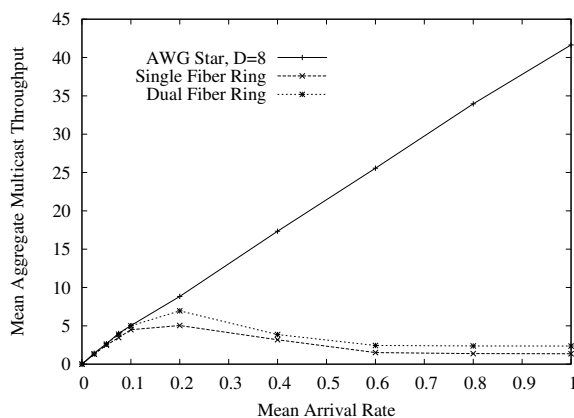


Fig. 58. Aggregate multicast throughput for uniform self-similar traffic with $p_m = 30\%$ multicast traffic

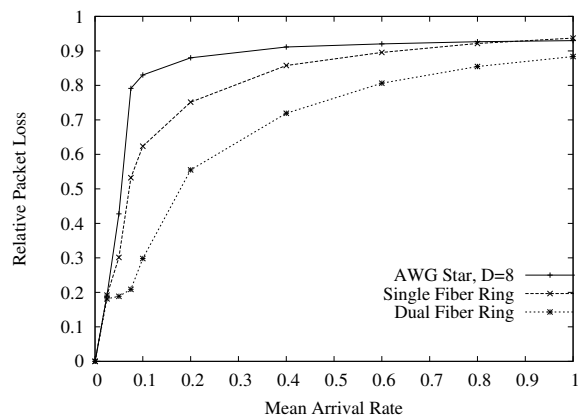


Fig. 59. Relative packet loss for uniform self-similar traffic with $p_m = 30\%$ multicast traffic

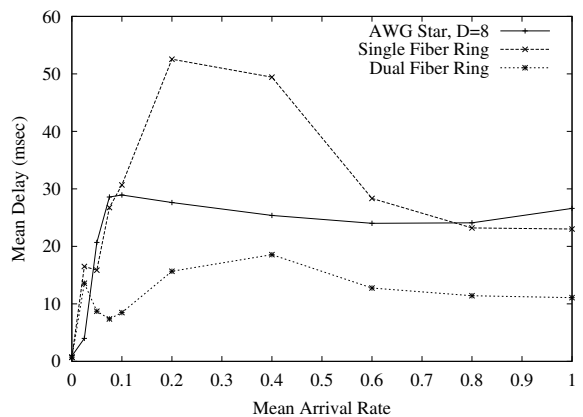


Fig. 60. Mean delay for uniform self-similar traffic with $p_m = 30\%$ multicast traffic

intended receivers at a given splitter to be free in the same slot. Therefore, the scheduling of multicast packets becomes difficult, especially as the traffic load increases. As a consequence, at high traffic loads the star network tends to transmit unicast packets (and a few multicast packet copies with a small number of destination nodes). (In ongoing work we are addressing this bias against multicast packets, one strategy is to partition the intended receivers at a splitter into subgroups.) The unicast packets are transmitted with moderate delay as they tend to experience some delay until they are selected in the buffer selection, but are then quickly scheduled. The few multicast packet copies that do eventually succeed in the scheduling, however, experience a very large delay. As a result the average delays are significantly larger for the mix of unicast and multicast traffic in the star network (see Fig. 60) compared to the delays for unicast traffic (see Fig. 47).

In contrast, we observe that the delays for the mix of unicast and multicast traffic in the ring networks (see Fig. 60) are smaller than the corresponding delays for unicast traffic (see Fig. 47). This is because multicast packet copies (especially those with many destinations) are given priority in the buffer selection as explained above and thus tend to experience relatively small queue build-up and queuing delays. At the same time, multicast packets with many destinations have a large impact on the average packet delay in the network, resulting in the small delays observed in Fig. 60.

Overall, we observed from Fig. 60 that the dual-fiber ring network gives the smallest delays. The delays in the star network are roughly twice as large for a wide range of traffic loads. In the single-fiber ring network there is a hump in the delay for moderate traffic loads (with roughly $0.2 \leq \sigma \leq 0.6$), which is due to the fact that the transmission of unicast packets that have experienced relatively large delays are rarely done. In single-fiber ring network, multicast data has priority over unicast data as σ increases as discussed above. Thus as σ increases, the more multicast data are sent. Fig. 58 reconfirms this. From the point $\sigma = 0.2$, multicast throughput decreases. By the definition of multicast throughput, this means that the more multicast data are sent and the less unicast data are sent. Generally, unicast data suffer large delay due to the low priority of unicast data. Thus the delay in single-fiber ring network decreases from $\sigma = 0.2$.

Generally, we may conclude that for multicast traffic the ring networks have the advantage that there are no receiver conflicts. A multicast packet copy that is transmitted in an empty slot is delivered to all its intended destinations around the ring without requiring any coordination of the receivers. In contrast in the TT-TR star network, destination conflicts tend to make the scheduling of multicast packet copies difficult. As we have observed in this section, the combination of these effects results in a significantly improved performance of the dual-fiber ring network over the star network. Throughout this section we focused on the aggregate network performance for mixed unicast and multicast traffic. As we noted in the interpretations of our results, unicast and multicast traffic experience different dynamics in the considered networks with the ring networks having a bias in favor of multicast traffic and the star network having a bias in favor of unicast traffic. In ongoing work we study the fair treatment of these traffic types.

V. CONCLUSION

We have compared the performance of state-of-the-art WDM star and WDM ring metro networks. We considered the AWG based star network with a TT–TR node architecture, as well as the all-optical single-fiber ring with TT–FR nodes and the counter-directional dual-fiber ring with a TT²–FT² node structure. In addition, fixed-tuned transceivers (FT–FR) are used in the ring networks for the transmission of control information over the control channel and for the out-of-band signalling in the AWG star network. We considered WDM ring networks with a slotted time structure and with the ATMR fairness control.

Our main finding is that the AWG star network with out-of-band signalling clearly outperforms the ring networks in terms of throughput, packet loss, and delay for unicast traffic. In addition, the star’s reservation protocol naturally provides fairness and support for variable-size packets. However, the dual-fiber ring network outperforms the AWG based star network for multicast traffic. As an architecture being relatively new to the metro area, future research should focus on solving the technological challenges of the AWG based star network to get closer to the market. For example, fast-tunable receivers are not yet commercially available, a cost efficient external control channel is required, and cost-effective protection strategies need to be developed.

All-optical WDM ring networks, on the other hand, have proven to be technically feasible in various testbeds. The dual fiber infrastructure from existing SONET based solutions can probably be reused for a cost-effective upgrade to the all-optical dual fiber ring, also featuring protection. Furthermore, techniques for accommodating variable-size packets in WDM ring networks are being studied, see for instance [9], and comparing them with the transport of variable-size packets in the star networks is an interesting avenue for future work. To be competitive with the star in terms of performance, future research should focus on developing new architectures allowing for a higher degree of spatial wavelength reuse.

In hot-spot traffic scenarios both the ring and the star’s performance is mostly limited by the capacity of the hot-spot’s transceivers. This requires special attention in the design of the access protocol and the node structure.

REFERENCES

- [1] P.-H. Ho and H. T. Mouftah, “A Framework of Scalable Optical Metropolitan Networks for Improving Survivability and Class of Service,” *IEEE Network*, vol. 16, no. 4, pp. 29–35, July/Aug. 2002.
- [2] B. Mukherjee, “WDM Optical Communication Networks: Progress and Challenges,” *IEEE Journal on Selected Areas in Communications*, vol. 18, no. 10, pp. 1810–1824, Oct. 2000.
- [3] M. Herzog, M. Maier, and M. Reisslein, “Metropolitan Area WDM Networks: A Survey on Ring Systems,” June 2003, submitted, available at <http://www.fulton.asu.edu/~mre>.
- [4] B. Mukherjee, “WDM–Based Local Lightwave Networks Part I: Single–Hop Systems,” *IEEE Network*, vol. 6, no. 3, pp. 12–27, May 1992.
- [5] M. Maier, M. Reisslein, and A. Wolisz, “Towards Efficient Packet Switching Metro WDM Networks,” *Optical Networks Magazine*, vol. 3, no. 6, pp. 44–62, Nov. 2002.
- [6] A. M. Hill, M. Brierley, R. M. Percival, R. Wyatt, D. Pitcher, K. M. I. Pati, I. Hall, and J.-P. Laude, “Multiple-Star Wavelength-Router Network and Its Protection Strategy,” *IEEE Journal on Selected Areas in Communications*, vol. 16, no. 7, pp. 1134–1145, Sept. 1998.
- [7] Y. Sakai, K. Noguchi, R. Yoshimura, T. Sakamoto, A. Okada, and M. Matsuoka, “Management System for Full–Mesh WDM AWG–Star Network,” in *Proceedings of The 27th European Conference on Optical Communication*, Sept. 2001, vol. 3, pp. 264–265.

- [8] C. Fan, M. Maier, and M. Reisslein, "The AWG||PSC Network: A Performance Enhanced Single-Hop WDM Network with Heterogeneous Protection," in *Proc. of IEEE Infocom '03*, San Francisco, Mar. 2003, pp. 2279–2289.
- [9] I. M. White, M. S. Rogge, K. Shrikhande, and L. G. Kazovsky, "Design of a Control-Based Media-Access-Control Protocol for HORNET," *Journal of Optical Networking*, vol. 1, no. 12, pp. 460–473, Dec. 2002.
- [10] C. S. Jelger and J. M. H. Elmirghani, "Photonic Packet WDM Ring Networks Architecture and Performance," *IEEE Communications Magazine*, vol. 40, no. 11, pp. 110–115, Nov. 2002.
- [11] J. Fransson, M. Johansson, M. Roughtan, L. Andrew, and M. A. Summerfield, "Design of a Medium Access Control Protocol for a WDMA/TDMA Photonic Ring Network," in *Proc., IEEE Globecom'98*, Nov. 1998, vol. 1, pp. 307–312.
- [12] R. Gaudino, A. Carena, V. Ferrero, A. Pozzi, V. D. Feo, P. Gigante, F. Neri, and P. Poggiolini, "RINGO: A WDM Ring Optical Packet Network Demonstrator," in *Proceedings of 27th European Conference on Optical Communication (ECOC 2001)*, Amsterdam, Netherlands, Oct. 2001, pp. 620–621.
- [13] J. Cai, A. Fumagalli, and I. Chlamtac, "The Multitoken Interarrival Time (MTIT) Access Protocol for Supporting Variable Size Packets Over WDM Ring Network," *IEEE Journal on Selected Areas in Communications*, vol. 18, no. 10, pp. 2094–2104, Oct. 2000.
- [14] I. Rubin and H.-K. H. Hua, "Synthesis and Throughput Behavior of WDM Meshed-Ring Networks Under Nonuniform Traffic Loading," *IEEE Journal of Lightwave Technology*, vol. 15, no. 8, pp. 1513–1521, Aug. 1997.
- [15] M. A. Marsan, A. Bianco, E. Leonardi, M. Meo, and F. Neri, "MAC Protocols and Fairness Control in WDM Multirings with Tunable Transmitters and Fixed Receivers," *IEEE Journal of Lightwave Technology*, vol. 14, no. 6, pp. 1230–1244, June 1996.
- [16] K. V. Shrikhande, I. M. White, D.-R. Wonglumsom, S. M. Gemelos, M. S. Rogge, Y. Fukushima, M. Avenarius, and L. G. Kazovsky, "HORNET: A Packet-Over-WDM Multiple Access Metropolitan Area Ring Network," *IEEE Journal on Selected Areas in Communications*, vol. 18, no. 10, pp. 2004–2016, Oct. 2000.
- [17] K. Bengi and H. R. van As, "Efficient QoS Support in a Slotted Multihop WDM Metro Ring," *IEEE Journal on Selected Areas in Communications*, vol. 20, no. 1, pp. 216–227, Jan. 2002.
- [18] M. Scheutzw, M. Maier, M. Reisslein, and A. Wolisz, "Wavelength reuse for efficient packet-switched transport in an AWG-based metro WDM network," *IEEE/OSA Journal of Lightwave Technology*, vol. 21, no. 6, pp. 1435–1455, June 2003.
- [19] M. Maier, M. Reisslein, and A. Wolisz, "A Hybrid MAC Protocol for a Metro WDM Network Using Multiple Free Spectral Ranges of an Arrayed-Waveguide Grating," *Computer Networks*, vol. 41, no. 4, pp. 407–433, Mar. 2003.
- [20] K. Kato, A. Okada, Y. Sakai, and K. Noguchi *et al.*, "10-Tbps Full-Mesh WDM Network Based On Cyclic-Frequency Arrayed-Waveguide Grating Router," in *Proc. of ECOC '00*, Munich, Germany, Sept. 2000, vol. 1, pp. 105–107.
- [21] A. Okada, T. Sakamoto, Y. Sakai, and K. Noguchi *et al.*, "All-Optical Packet Routing by an Out-of-Band Optical Label and Wavelength Conversion in a Full-Mesh Network Based on a Cyclic-Frequency AWG," in *Proc. of OFC 2001 Technical Digest, paper ThG5*, Anaheim, CA, Mar. 2001.
- [22] N. P. Caponio, A. M. Hill, F. Neri, and R. Sabella, "Single-Layer Optical Platform Based on WDM/TDM Multiple Access for Large-Scale 'Switchless' Networks," *European Trans. on Telecomm.*, vol. 11, no. 1, pp. 73–82, Jan./Feb. 2000.
- [23] A. Bianco, E. Leonardi, M. Mellia, and F. Neri, "Network Controller Design for SONATA — A Large-Scale All-Optical Passive Network," *IEEE Journal on Selected Areas in Communications*, vol. 18, no. 10, pp. 2017–2028, Oct. 2000.
- [24] M. Maier and A. Wolisz, "Demonstrating the Potential of Arrayed-Waveguide Grating Based Single-Hop WDM Networks," *Optical Networks Magazine*, vol. 2, no. 5, pp. 75–85, Sept. 2001.
- [25] I. Rubin and J. Ling, "Delay Analysis of All-Optical Packet-Switching Ring and Bus Communications Networks," in *Proc. of IEEE Globecom 2001*, Nov. 2001, vol. 3, pp. 1585–1589.
- [26] I. M. White, E. S.-T. Hu, Y.-L. Hsueh, K. V. Shrikhande, M. S. Rogge, and L. G. Kazovsky, "Demonstration and system analysis of the HORNET," *IEEE/OSA Journal of Lightwave Technology*, vol. 21, no. 11, pp. 2489–2498, Nov. 2003.
- [27] I. M. White, M. S. Rogge, K. V. Shrikhande, and L. G. Kazovsky, "A summary of the HORNET project: A next-generation metropolitan area network," *IEEE Journal on Selected Areas in Communications*, vol. 21, no. 9, pp. 1478–1494, Nov. 2003.
- [28] K. Shrikhande, A. Srivatsa, I. M. White, M. S. Rogge, D. Wonglumsom, S. M. Gemelos, and L. G. Kazovsky, "CSMA/CA MAC Protocols for IP-HORNET: An IP over WDM Metropolitan Area Ring Network," in *Proceedings of Globecom '00*, San Francisco, CA, Nov. 2000, vol. 2, pp. 1303–1307.
- [29] O. A. Lavrova, G. Rossi, and D. J. Blumenthal, "Rapid tunable transmitter with large number of ITU channels accessible in less than 5 ns," in *Proc. of ECOC '00*, Munich, Germany, Sept. 2000, vol. 2, pp. 169–170.
- [30] D.-R. Wonglumsom, I. M. White, K. V. Shrikhande, M. S. Rogge, S. M. Gemelos, F.-T. An, Y. Fukushima, M. Avenarius, and L. G. Kazovsky, "Experimental demonstration of an access point for HORNET—A Packet-Over-WDM Multiple-Access MAN," *IEEE/OSA Journal of Lightwave Technology*, vol. 18, no. 12, pp. 1709–1717, Dec. 2000.
- [31] M. Herzog, "Design und Untersuchung von optischen Metropolitan Area Networks (MANs) unter Berücksichtigung von neuen MAC Protokollen," Sept. 2002, Masters Thesis, Institute of Photonics, Technical University Berlin.
- [32] J. J. O. Pires, M. J. O'Mahony, N. Parnis, and E. Jones, "Size limitations of a WDM ring network based on arrayed-waveguide grating OADMs," in *Proceedings of IFIP International Conference on Optical Network Design and Modelling (ONDM)*, Paris, France, Feb. 1999, pp. 71–79.
- [33] J. J. O. Pires, M. J. O'Mahony, N. Parnis, and E. Jones, "Scaling limitations in full-mesh WDM ring networks using arrayed-waveguide grating OADMs," *IEEE Electronics Letters*, vol. 35, no. 1, pp. 73–75, Jan. 1999.
- [34] N. Antoniadis, K. Ennsner, V. L. da Silva, and M. Yadlowsky, "Computer simulation of a metro WDM ring network," in *Digest of the IEEE LEOS Summer Topical Meetings*, July 2000, pp. IV19–IV20.

- [35] H. I. Saleheen, "Impact of closed cycle ASE accumulation on optical network performance," in *Proceedings of 14th Annual Meeting of the IEEE Lasers and Electro-Optics Society (LEOS)*, Nov. 2001, pp. 32–33.
- [36] A. Yu, M. J. O'Mahony, and A. M. Hill, "Transmission limitation of all-optical network based on $N \times N$ multi/demultiplexer," *Electronics Letters*, vol. 33, no. 12, pp. 1068–1069, June 1997.
- [37] M. A. Marsan, A. Bianco, E. Leonardi, A. Morabito, and F. Neri, "All-optical WDM Multi-Rings with Differential QoS," *IEEE Communications Magazine*, vol. 37, no. 2, pp. 58–66, Feb. 1999.
- [38] M. Cerisola, T. K. Fong, R. T. Hofmeister, L. G. Kazovsky, C.-L. Lu, P. Poggiolini, and D.J.M. Sabido IX, "CORD — a WDM optical network: Control mechanism using subcarrier multiplexing and novel synchronization solutions," in *Proceedings of ICC '95*, Seattle, WA, June 1995, pp. 261–265.
- [39] I. Chlamtac, A. Fumagalli, L.G. Kazovsky, P. Melman, W.H. Nelson, P. Poggiolini, M. Cerisola, A.N.M.M. Choudhury, T.K. Fong, R.T. Hofmeister, C.-L. Lu, A. Mekkittikul, D.J.M. Sabido IX, C.-J. Suh, and E.W.M. Wong, "CORD: contention resolution by delay lines," *IEEE Journal on Selected Areas in Communications*, vol. 14, no. 5, pp. 1014–1029, June 1996.
- [40] R. T. Hofmeister, C.-L. Lu, M.-C. Ho, P. Poggiolini, and L. G. Kazovsky, "Distributed slot synchronization (DSS): A network-wide slot synchronization technique for packet-switched optical networks," *IEEE/OSA Journal of Lightwave Technology*, vol. 16, no. 12, pp. 2109–2116, Dec. 1998.
- [41] R. Ramaswami and K. Sivarajan, *Optical Networks: A Practical Perspective*, Morgan Kaufmann, 2002.
- [42] K. Park and W. Willinger, Eds., *Self-Similar Network Traffic and Performance Evaluation*, John Wiley & Sons Inc., 2000.
- [43] I. Cidon and Y. Ofek, "MetaRing – A Full-Duplex Ring with Fairness and Spatial Reuse," *IEEE Transactions on Communications*, vol. 41, no. 1, pp. 110–120, Jan. 1993.
- [44] J. Chen, I. Cidon, and Y. Ofek, "A Local Fairness Algorithm for the MetaRing and its performance study," *IEEE Journal of Selected Areas in Communications*, vol. 11, pp. 1183–1192, Oct. 1993.
- [45] K. Imai, T. Ito, H. Kasahara, and N. Morita, "ATMR: Asynchronous Transfer Mode Ring Protocol," *Computer Networks and ISDN Systems*, vol. 26, pp. 785–798, Mar. 1994.
- [46] C. Zhou and Y. Yang, "Wide-sense Nonblocking Multicast in a Class of Regular Optical WDM Networks," *IEEE Trans. on Comm.*, vol. 50, no. 1, pp. 126–134, Jan. 2002.
- [47] M. Maier, M. Scheutzow, and M. Reisslein, "The Arrayed-Waveguide Grating Based Single-Hop WDM Network: An Architecture for Efficient Multicasting," Tech. Rep., Arizona State University, Telecommunications Research Center, available at <http://www.fulton.asu.edu/~mre>, Dec. 2002.